Katabatic and convective processes drive two preferred peaks in the precipitation diurnal cycle over the Central Himalaya

Hunt, K. M. R. ORCID: https://orcid.org/0000-0003-1480-3755, Turner, A. G. ORCID: https://orcid.org/0000-0002-0642-6876 and Schiemann, R. K. H. ORCID: https://orcid.org/0000-0003-3095-9856 (2022) Katabatic and convective processes drive two preferred peaks in the precipitation diurnal cycle over the Central Himalaya. Quarterly Journal of the Royal Meteorological Society, 148 (745). pp. 1731-1751. ISSN 1477-870X doi: https://doi.org/10.1002/qj.4275 Available at https://centaur.reading.ac.uk/104198/

Received: 25 October 2021 | Revised: 9 February 2022 | Accepted: 18 March 2022

DOI: 10.1002/qj.4275

Quarterly Journal of the Royal Meteorological Society RMetS

RESEARCH ARTICLE

Katabatic and convective processes drive two preferred peaks in the precipitation diurnal cycle over the Central Himalaya

Kieran M. R. Hunt[1,2] | **Andrew G. Turner**[1,2] | **Reinhard K. H. Schiemann**[1,2]

[1]Department of Meteorology, University of Reading, Reading, UK

[2]National Centre for Atmospheric Science, University of Reading, Reading, UK

Correspondence
K. M. R. Hunt, Department of Meteorology, Whiteknights Campus, University of Reading, RG6 6BB, UK.
Email: k.m.r.hunt@reading.ac.uk

Funding information
Newton Fund/Indian Ministry of Earth Sciences, Grant/Award Number: WCSSP Lot3 WP2

Abstract

The diurnal cycle of precipitation over the Central Himalaya is governed by a complex interaction between the diurnal cycle of tropical convection and local orographic flow. Understanding this interaction is crucial for model evaluation, where the simulation of such processes is highly sensitive to model resolution and choice of parametrisation schemes. In this study, the mean diurnal cycle is computed using gridded satellite data–Integrated Multi-satellitE Retrievals for *Global Precipitation Measurement (GPM)* (IMERG) data and is shown to be bimodal, with one peak in the late afternoon (1700 India Standard Time (IST)) and a stronger one in the early morning (0200 IST). This structure is an artefact of compositing, as individual days are associated with single peaks. The late-afternoon "convective" peak is shown to be linked to the diurnal cycle of tropical convection, whereas the nocturnal "katabatic" peak is shown to be triggered by nocturnal downslope flow converging with the background monsoon circulation. As such, the katabatic peak is strongly favoured by an active monsoon trough, which provides greater southeasterly moisture flux to the foothills, resulting in increased low-level moisture flux convergence upon interaction with the katabatic northerlies. When the trough is less active, precipitation is brought to the region by mesoscale convective systems, ranging in scale from tens to thousands of kilometres, resulting in convective peaks. We hypothesise that these convective afternoon peaks are enhanced by anabatic flow. It is shown that the Boreal Summer Intraseasonal Oscillation does not play a significant role in modulating either the timing or the amplitude of the diurnal cycle; however, low-pressure systems do: either by intensifying the trough (and hence the katabatic peak), or, when further north, by providing deep convection (hence supporting the convective peak). Two reanalyses and a separate 17-km model with parametrised convection capture both peaks, but overestimate the magnitude of the convective peak and underestimate the magnitude of the katabatic peak.

KEYWORDS

Central Himalaya, deep convection, diurnal cycle, orographic processes, precipitation

1 | INTRODUCTION

Over much of monsoonal India, the diurnal cycle of precipitation is dominated by tropical convection (Yang and Slingo, 2001): solar heating warms the surface, which then warms and moistens the boundary layer through sensible and latent heat transfer. Eventually, the updrafts become strong enough to overcome convective inhibition and, by the late afternoon, deep convection is widespread (e.g., Wallace, 1975). This picture gets increasingly complicated near the coasts, where the land–sea breeze plays an important secondary role, and near the Himalaya, where localised dynamics such as the nocturnal jet can alter atmospheric stability dramatically (Nesbitt and Zipser, 2003; Sen Roy and Balling, 2007). It is this latter problem that is the focus of this study.

A full understanding of the processes at play, and how they interact with each other to produce the observed diurnal cycle across the Himalaya, is vital for model evaluation. In particular, parametrisation of these localised processes (e.g., to represent convection or subgrid orography) can lead to significant biases even on the synoptic scale. Marsham *et al.* (2013) showed that, in simulations of the West African monsoon, parametrised convection occurred too early in the day, leading to mistimed feedbacks between radiative heating, latent heating, and the meridional pressure gradient. This resulted in a much poorer simulation of the monsoon circulation than a parallel run with explicit convection. More generally, coarse-resolution models with parametrised convection tend to rain too early in the Tropics and this premature initiation suppresses the build-up of convective available potential energy (CAPE), resulting in too light and too frequent precipitation over tropical land, with similar implications for the simulation of monsoonal circulation (Dai and Trenberth, 2004).

1.1 | The observed diurnal cycle of precipitation over the Himalaya

Satellite-based precipitation products have allowed a near-global assessment of the diurnal cycle of precipitation. Kikuchi and Wang (2008) showed that the strongest diurnal cycle exists over tropical land, where the peak (at 1500 local solar time, or LT) usually matched local heating. They also found that near large mountain ranges the peak tended to be in the local early morning. This was corroborated by Sahany *et al.* (2010), who used spectral analysis to draw out the diurnal cycle over nine years of *Tropical Rainfall Measuring Mission* (*TRMM*) data over India. They found that inland, away from the coasts or orography, the precipitation peaked at 1430 LT; however, this occurred later over the Western Ghats (1430–1730 LT) and much earlier over the Himalayan foothills, where they recorded a single peak at 0230 LT. More recently, Watters *et al.* (2021) expanded these results for *Global Precipitation Measurement* (*GPM*)–Integrated Multi-satellitE Retrievals for *GPM* (IMERG), ECMWF Reanalysis v5 (ERA5), and three Coupled Model Intercomparison Project Version 6 (CMIP6) Atmospheric Model Intercomparison Project (AMIP) models. They found that IMERG also captured an early-morning precipitation maximum over the Himalaya, with a cross-slope gradient (earlier maximum at higher altitudes), as well as a late-afternoon maximum both further south (over the Indo-Gangetic Plain) and further north (over the Tibetan Plateau). The ERA5 reanalysis was able to capture most of these features, but had a late-afternoon peak over much of the Himalaya.

More directed studies, combining satellite data with ground-based observations, have reached similar conclusions. Barros *et al.* (2000) explored the diurnal cycle of precipitation over Nepal for a single monsoon season. They found that the diurnal cycle was often bimodal, with a late-afternoon and an early-morning peak, though in the valleys only the early-morning peak was present. This was later complemented by a longer radiosonde campaign (Barros and Lang, 2003). Similarly, Bhatt and Nakamura (2006) explored the diurnal cycle over the Himalayas in a range of data sources, finding a mid-afternoon peak in the pre-monsoon and an early-morning peak during the monsoon.

1.2 | Proposed mechanisms

Fitzjarrald (1984) constructed a one-dimensional model of katabatic winds in an ambient flow. He found that the onset time of katabatic (i.e., nocturnally forced downslope) winds is sensitive to opposing flow and reduced cooling rates (e.g., from monsoon cloudiness). Over the Central Himalaya, the katabatic winds are northerly, and the opposing flow is thus the local southeasterly monsoonal circulation. The model had about an eight hour delay between sunset and the initiation of katabatic flow over humid tropical slopes, but, because it was one-dimensional, missed the effects of local convergence due to local topography. He also found that entrainment into katabatic winds might be an important control on downslope initiation of precipitation. Bluestein (1993) suggested that the nocturnal low-level jet that arises in response to differential heating/cooling across the orographic gradient could advect moisture into such a region, causing the early-morning precipitation maximum seen in the Rockies. Using an intensive sonde and observation campaign over central Nepal and supported by reanalysis

data, Barros and Lang (2003) found that precipitable water peaked around midnight, slightly after CAPE. They found that anabatic winds were more intense than katabatic winds, in agreement with many previous studies (Egger *et al.*, 2000; Ueno *et al.*, 2001; Bollasina *et al.*, 2002, as well as Fitzjarrald, 1984), as climatological monsoon winds are directed slightly upslope. They argued that convergence along the foothills was reduced during the day because of anabatic flow, favouring increased convergence at night (when the flow was katabatic). This way, as the monsoon continues to moisten the boundary layer, instability builds up during the whole day before it is finally released during the nocturnal precipitation. A similar argument was made by Houze *et al.* (2007), who suggested that deep convection near the Himalaya might be triggered by diurnal processes interacting with the monsoon circulation. Barros and Lang (2003) found little evidence of a nocturnal low-level jet, but noted that this may have been due to the data sparsity of the region. Ahrens *et al.* (2020), however, did find a nocturnal jet, but found that it did not contribute to triggering convection. Bhatt and Nakamura (2006) analysed the diurnal cycle using a combination of *TRMM*, radiosonde data, and two reanalyses. Following Fitzjarrald (1984), they attributed the early-morning maximum to convergence from the interaction between katabatic flow and the southeasterly moisture flux of the summer monsoon. They further suggested that cloud-top radiative cooling may be an important driver and found that the cross-slope gradient in peak timing could be explained by cold-pool density currents moving downslope, causing southward movement of precipitation systems in the morning. They also hypothesised that convection over the foothills could be triggered by gravity waves generated in response to the Himalaya acting to block the monsoon flow, arguing that this effect would be strongest in the early morning. Indeed, Rüthrich *et al.* (2013) found that maximum cloudiness over the Central Himalayan foothills occurred at 0200 LT, but hypothesised that this was due to katabatic flow helping initiate mesoscale convective systems. Using a different approach, Medina *et al.* (2010) attributed differences in the morphology of convective storms in the West and East Himalaya to the markedly different diurnal cycles of surface heat fluxes between the Thar Desert and the wetlands of Bangladesh.

Other studies have also investigated satellite-derived cloud data or high-resolution models over the Himalaya to improve understanding of the diurnal cycle. Barros *et al.* (2004) found a strong link between cloudiness and precipitation over the Himalaya at all scales, from the synoptic, which they linked to mesoscale convective systems (MCSs) and monsoon depressions, to the mesoscale, which they linked to valleys and ridges in the orography. They found that the timing of heavy precipitation over the Himalaya was driven by variability on the synoptic scale (which they defined as larger than 70 km), although convective cloud clusters are comparatively rare there compared with the Indo-Gangetic Plain and the Tibetan Plateau. Analysing extreme convection over the whole of South Asia, using the *TRMM* precipitation radar, Romatschke *et al.* (2010) found that different types of organised convection have differing diurnal cycles: deep convective cores peak at about 1700 LT, wide convective cores peak at either 1700–1800 LT or 0300–0400 LT, and broad stratiform regions have a weak diurnal cycle that peaks at about 0600 LT. Romatschke and Houze (2011) investigated this further over the Central Himalayan foothills, concluding that small and medium sized (<44,000 km^2) convective systems develop as the monsoon flow is forced upslope, and that medium-sized systems were triggered at lower elevations by katabatic flow. Ahrens *et al.* (2020) found that the simulation of the diurnal cycle was vastly improved by moving from a regional climate model with parametrised convection and a horizontal resolution of 20 km to a high-resolution model with explicit convection and a horizontal resolution of 2.8 km, attributing this improvement to improved representation of both convection and orography. They found that both long-lived convective systems and the convergence of katabatic and monsoonal flows played a role in supporting the diurnal cycle. Norris *et al.* (2017) found a similar improvement in moving from parametrised to explicit convection, though there was no significant improvement in improving the resolution thereafter from 6.7 to 2.2 km. They found that their simulated diurnal cycle was elevation-dependent, with a bimodal cycle (peaks at 0600 and 2100 LT) below 3 km and a unimodal cycle (peak at 1500 LT) above 3 km. The simulation with parametrised convection was unable to capture the nocturnal (0600 LT) peak at lower elevations. Using dynamical downscaling, they later showed (Norris *et al.*, 2020) that climate change had amplified the diurnal cycle over the last 36 years, as increased warming of the slopes during the daytime and clearer skies and increased radiative cooling at night enhanced the anabatic and katabatic winds, respectively.

1.3 | Aims and outline

In this article, we intend to disentangle the bimodal structure of the diurnal cycle over the Central Himalaya, to investigate the respective roles of katabatic and convective processes, and to understand how these processes interact with each other and whether forcing from large-scale modes of intraseasonal variability offers additional predictability for precipitation over the Central Himalaya.

We outline the data and methods used in Section 2. The results are discussed in Section 3: the diurnal cycle is investigated and decomposed in Section 3.1, the synoptic-scale elements associated with each component are explored in Section 3.2, and responsible modes of intraseasonal variability are discussed in Section 3.3. Finally we discuss the implications of our results in Section 4 and conclude in Section 5.

2 | DATA AND METHODS

2.1 | Data

2.1.1 | *GPM*–IMERG

For our precipitation dataset, we use the gridded surface product IMERG (Huffman *et al.*, 2015). This has global coverage at a half-hourly, 0.1° resolution, starting in June 2000 and continuing to the present day. Over the Tropics, IMERG primarily ingests retrievals from (for 2000–2014) the now-defunct *Tropical Rainfall Measuring Mission* (*TRMM*: Kummerow *et al.*, 1998; 2000) 13.8-GHz precipitation radar and microwave imager (Kozu *et al.*, 2001) and (for 2014 onwards) the *Global Precipitation Measurement* (*GPM*: Hou *et al.*, 2014) Ka/Ku-band dual-frequency precipitation radar. When an overpass is not available, precipitation is estimated by calibrating infrared measurements from geostationary satellites. While *GPM*–IMERG performs well when compared against gauge-based products, performance falls at higher elevations or when quantifying extreme precipitation events (Prakash *et al.*, 2018), although it performs well over the Western Himalaya (Baudouin *et al.*, 2020). IMERG has good skill in capturing the diurnal cycle over the Tropics and subtropics: for example, for Africa (Dezfuli *et al.*, 2017) and China (Tang *et al.*, 2020). To check whether the change in core observations from *TRMM* precipitation radar to *GPM* precipitation radar affected the *GPM*–IMERG diurnal cycle, we compared statistics and spatial maps for both periods (not shown), but found no significant difference between the two.

2.1.2 | CMORPH

The Climate Prediction Center morphing method (CMORPH) (Joyce *et al.*, 2004) is also a multisatellite precipitation dataset, though, unlike *GPM*–IMERG, it does not undergo a gauge calibration adjustment process. It is available at hourly, $0.1° \times 0.1°$ resolution from 2000 onwards. We use CMORPH as an alternative to *GPM*–IMERG to replicate results and quantify uncertainty. Data were downloaded from ftp://ftp.cpc.ncep.noaa.gov/precip/global_CMORPH/3-hourly_025deg/. CMORPH, along with the *TRMM* Multi-satellite Precipitation Analysis (TMPA, the predecessor of *GPM*–IMERG), replicates the diurnal cycle well in tropical Africa compared with gauge data (Pfeifroth *et al.*, 2016); however, the peaks in satellite data are often delayed by about an hour compared with gauges, which the authors attribute to (a) the delay between maximum precipitation and minimum cloud-top temperature and (b) biases associated with advection of the associated anvils.

2.1.3 | *Kalpana* OLR

To identify regions of deep convection, we use gridded outgoing longwave radiation (OLR) derived from the very-high resolution radiometer on board the *Kalpana* satellite (Singh *et al.*, 2007; Mahakur *et al.*, 2013). The data are available from 2004–2017 at three-hourly, $0.25° \times 0.25°$ resolution from 40°S–40°N and 25°E–125°E. Data are curated by the Indian Institute of Tropical Meteorology and were downloaded from https://www.tropmet.res.in/~mahakur/Public_Data/index.php?dir=K1OLR/3Hrly.

2.1.4 | ERA5

To investigate the local and synoptic-scale structure of the boundary layer and troposphere, we use data from the European Centre for Medium-Range Weather Forecasts (ECMWF) ERA5 reanalysis (Hersbach *et al.*, 2020). Data are available globally, at hourly resolution from 1950 onwards, on a $0.25° \times 0.25°$ grid. Data are available over 37 pressure levels from 1,000 to 0.01 hPa, as well as at selected heights above the surface. Data are assimilated into the forecasting system from a large variety of sources, including satellites, automatic weather stations, and radiosondes. The resolution of the underlying model means that convection is parametrised. Data were downloaded from the Copernicus Data Store: https://cds.climate.copernicus.eu/cdsapp#!/dataset/reanalysis-era5-pressure-levels?tab=overview.

2.1.5 | IMDAA

The Indian Monsoon Data Assimilation and Analysis (IMDAA) project is a regional analysis available at 12 km resolution, covering India and the surrounding region from 1979–2018. Key differences from ERA5 are the underlying model (IMDAA uses the UK Met Office Unified Model; ERA5 uses the ECMWF Integrated Forecast System) and the assimilated data (IMDAA includes

more surface and upper-air observations). Like ERA5, the underlying model resolution requires parametrised convection. Data were downloaded from the dedicated NCMRWF server: https://rds.ncmrwf.gov.in/.

2.1.6 | LPS tracks

We use the database of low-pressure system (LPS) tracks from Hunt and Fletcher (2019) in this study. Using six-hourly ERA-Interim data, they tracked LPSs by computing the mean relative vorticity in the 900–800 hPa layer, then performing a spectral truncation at T63 to filter out short-wavelength noise. They then identified regions of positive relative vorticity within this field and determined the centroid location for each one. These centroids were then linked in time, subject to constraints in distance and steering winds, to form candidate LPS tracks. This algorithm has been used for monsoon LPSs by a number of authors (e.g., Arulalan *et al.*, 2020; Dong *et al.*, 2020; Martin *et al.*, 2020). Track data are available from https://doi.org/10.5281/zenodo.5575336.

2.1.7 | BSISO indices

Data for the Boreal Summer Intraseasonal Oscillation (BSISO) were downloaded from http://iprc.soest.hawaii.edu/users/kazuyosh/Bimodal_ISO.html, the methodology of which is described in Lee *et al.* (2013). They are used to assess the role of large-scale intraseasonal variability in modulating the diurnal cycle of precipitation over the Himalayas. The dataset has daily resolution, available from 1979–2018. It contains the normalised values of the first two principal components (or RMMs), as well as the resulting phase and amplitude.

2.2 | Methods

2.2.1 | Choice of study region

This study is concerned with the diurnal cycle along the foothills and Himalaya. However, this is a broad region and the synoptic conditions in the western Himalaya are often very different from those in the east. We therefore select a representative study region, over which the dynamics will be locally coherent, but which can still capture the range of processes governing the diurnal cycle in both the foothills and mountains of the Central Himalaya. To this end, using data shown in Figure 1 we choose the box (82–83°E, 28–30°N). This is in the Central Himalaya, which feels the full force of the summer monsoon between July and August. The study region contains surface elevations ranging from ~200 m in its southwest to over 6,000 m in its northeast, and has a footprint much smaller than the typical length scale of the synoptic-scale dynamics that typically dominate the region. It also has no significant valleys or bodies of water, but captures the band of steep orographic gradient that stretches along the Central Himalaya. Figure 2 shows high-resolution orography for the study region from Earth Topography (ETOPO1) (https://www.ngdc.noaa.gov/mgg/global/global.html).

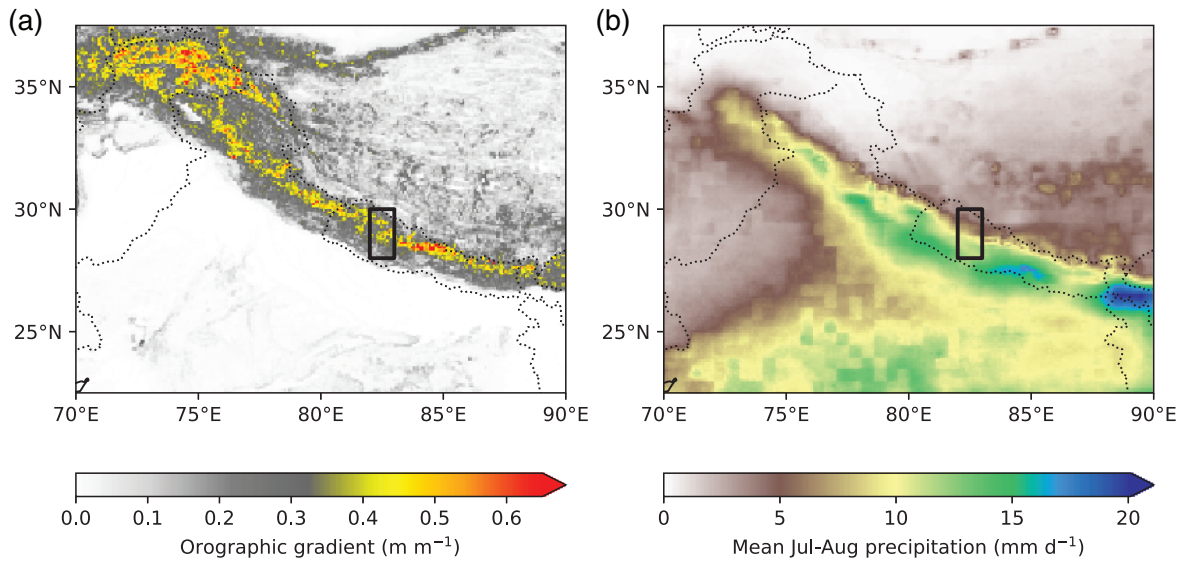

FIGURE 1 The environment of the Central Himalayan foothills. (a) Orographic gradient (m m^{-1}) computed using ETOPO1, regridded to 8 km using a maximum filter. (b) Mean July–August precipitation (mm · day^{-1}) computed using *GPM*–IMERG data (2000–2019). In each panel, the study region is marked by a black rectangle [Colour figure can be viewed at wileyonlinelibrary.com]

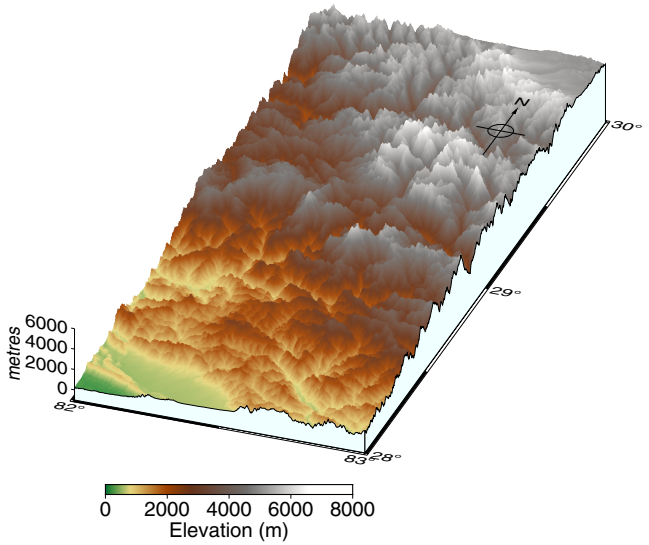

FIGURE 2 Orography of the study region [82–83°E, 28–30°N] in the Central Himalaya. Data from ETOPO1[Colour figure can be viewed at wileyonlinelibrary.com]

Unless stated otherwise, throughout the article, averages and climatologies are computed for July and August, when the monsoon fully covers the Himalaya. We use Indian Standard Time (IST: UTC + 0530) throughout the study, with occasional reference to UTC to aid the reader while maintaining a standardised time format. Where phrases such as "morning", or "late afternoon" are used, this always refers to the local time.

2.2.2 | Circular standard deviation

When dealing with angular data (such as hours of the day), the conventional standard deviation is inadequate, as it does not handle the discontinuity at 2π appropriately. To compute the circular or "directional" standard deviation, we use the following calculation (Fisher, 1995) for a one-dimensional series a with cycles of length Ω:

$$S = \frac{1}{n}\sum_{1}^{n} \sin\left(\frac{2\pi}{\Omega}a_n\right), \qquad C = \frac{1}{n}\sum_{1}^{n} \cos\left(\frac{2\pi}{\Omega}a_n\right), \quad (1)$$

then the circular variance, R, is given by

$$R = \sqrt{S^2 + C^2}, \quad (2)$$

and hence the circular standard deviation is

$$\sigma_c = \Omega \cdot \sqrt{(-2\log R)}\,. \quad (3)$$

For the diurnal cycle, $\Omega = 24$ hr.

3 | RESULTS

3.1 | Disentangling the diurnal cycle

We start by quantifying the diurnal cycle in a range of satellite and reanalysis products, before using composite synoptic charts and vertical cross-sections to quantify the underlying processes.

An overview of the diurnal cycle of monsoon precipitation in two satellite products (*GPM*–IMERG and CMORPH) and two reanalysis products (ERA5 and IMDAA) is given in Figure 3. Here, the peak time of the diurnal cycle is computed by creating the mean diurnal cycle of July–August precipitation at each pixel in each dataset and then identifying the time of the maximum value of that cycle. The two satellite products bear a strong similarity and highlight several key features. First, along the region of steepest orographic gradient (from the foothills to the peaks), stretching from the east to the west Himalaya, the peak precipitation occurs predominantly during early local morning (0300 IST). Within this "foothill" band is a slight meridional gradient, such that the peak precipitation at its southern boundary occurs 1–2 hr later than at the northern boundary. The foothill band is also punctuated, particularly in *GPM*–IMERG, by smaller regions where the peak precipitation occurs in the local late afternoon (1800 IST), which are collocated with larger valleys embedded within the foothills. To the south of the foothills lies the Indo-Gangetic Plain, for which both satellite datasets agree that the peak monsoon precipitation occurs in the local mid-afternoon (1500 IST), about 12 hr apart from the peak activity in the foothills. This is consistent with the diurnal cycle of tropical convection, and varies little in this region, although both *GPM*–IMERG and CMORPH agree that it occurs a little earlier in the north and up to a few hours later towards the southwest (Gujarat). Finally, north of the foothills and the Himalaya, lies the Tibetan Plateau. This is a region of comparatively low precipitation and the satellite datasets disagree here more than in any other region, although both suggest that precipitation peaks generally in local mid or late afternoon.

The two reanalyses show a mixed ability to capture this regional variability. Over the plains, ERA5 puts the diurnal peak, correctly, in the mid-to-late local afternoon but does not capture the subtle meridional gradient. Regardless, this is a significant improvement over earlier reanalyses and IMDAA, the parametrisation schemes of which tended to prefer triggering tropical convection at local noon (Dai and Trenberth, 2004; Dirmeyer *et al.*, 2012). The reanalyses both appear to extend the tropical convection signal northward over the foothills, placing

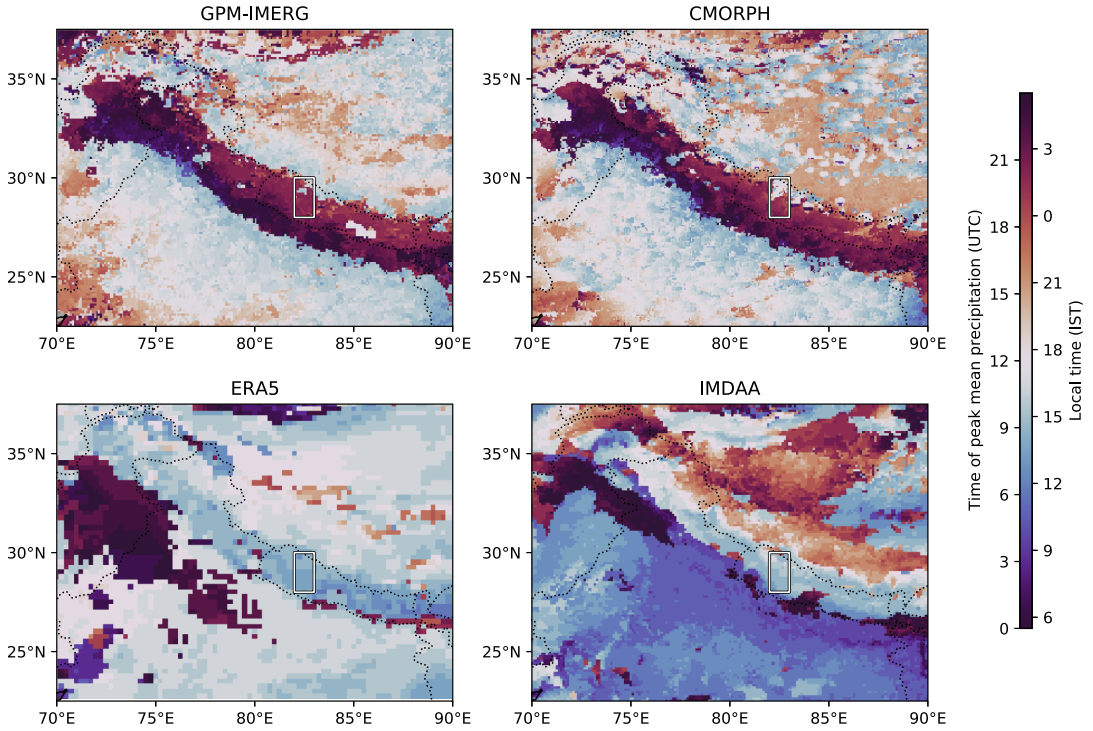

FIGURE 3 Time of the peak of the mean diurnal cycle of July–August precipitation over the Himalayas computed for selected datasets. Top: *GPM*–IMERG and CMORPH are primarily satellite-based products. Bottom: ERA5 and IMDAA are high-resolution reanalyses with parametrised convection. The study region is marked by a white rectangle[Colour figure can be viewed at wileyonlinelibrary.com]

a mid-afternoon peak along much of the region, at odds with the two satellite-based datasets. Early-morning peaks are only present, for both reanalyses, towards the far northwest and at small, isolated locations along the very southern boundary. It is interesting that, despite having different underlying models—ERA5 uses the ECMWF IFS and IMDAA uses the Met Office Unified Model—and assimilating different data, the two reanalyses suffer similar errors along the foothills. In the western Himalaya, where monsoon precipitation is weak (see Figure 1), this error can be explained by the tendency of the models to produce too much convective precipitation or advect it too far north. This bias would likely disappear should the nocturnal dynamics cause the observed early-morning peak to take over. Over the Tibetan Plateau, ERA5 captures the broad mid-to-late-afternoon peak, but IMDAA has significant difficulty, tending to place precipitation around local midnight, but with a large spatial variability. Model precipitation here is typically produced by the underlying large-scale microphysics schemes (Sharma *et al.*, 2021), and so is perhaps not related to IMDAA's convective scheme, rather the fact that it assimilates substantially fewer observations from outside India than does ERA5 (Rani *et al.*, 2021).

Figure 4 shows some characteristics of the diurnal cycle over the study region (82–83°E, 28–30°N; see Section 2.2.1) according to *GPM*–IMERG. Precipitation here is not marked by a single nocturnal peak, but instead by two distinct peaks: one in mid-afternoon centred at 1500–1600 IST and a larger one just after local midnight centred at 0200–0300 IST. This suggests a greater complexity to the processes underlying the diurnal cycle than analysis of the satellite data in Figure 3 first suggested, although the nature of the reanalysis errors hinted that more than one mechanism may be at play. The peaks have approximately equal magnitude when the median diurnal cycle is considered, implying a longer tail in the nocturnal distribution (i.e., populated by comparatively heavier precipitation events). Both peaks are broad, as well, suggesting that either the precipitation events involved have a reasonable duration and/or the timing of the trigger mechanisms can vary from day to day. We will explore this further in Figure 5.

The diurnal cycle changes throughout the year, as well. When the monsoon is undergoing onset or withdrawal (June and September), it is considerably less active over the Himalaya. During this period, the earlier, mid-afternoon peak has a higher mean than the nocturnal peak—indicating that the underlying mechanisms respond differently to the cloudiness and moisture brought by the presence of an active monsoon trough, the northern edge of which can often reach the foothills. The post-monsoon season (October–November) has a very similar pattern to June and September, though

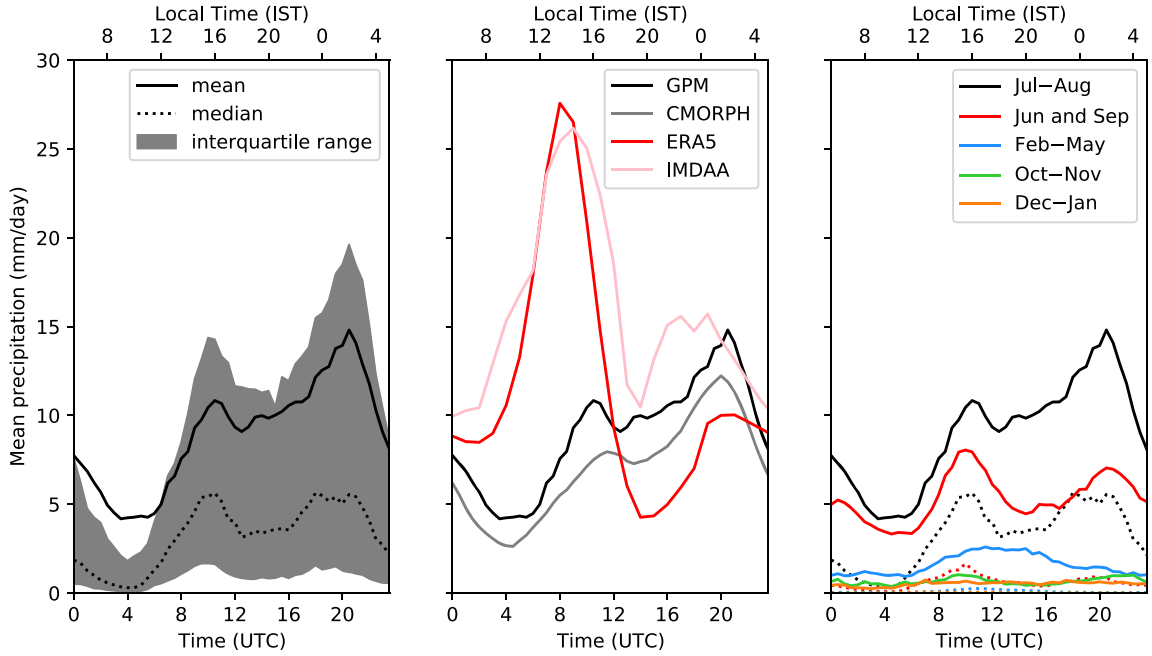

FIGURE 4 The diurnal cycle of precipitation over the study region (82–83°E, 28–30°N). Left: the mean (solid black), median (dotted black), and interquartile range (grey) of the diurnal cycle in July and August, computed using *GPM*–IMERG data from 2000–2020. Centre: the mean diurnal cycle for the same period for different datasets. Right: the mean (solid) and median (dotted) diurnal cycles for selected seasons, computed using *GPM*–IMERG data from 2000–2020[Colour figure can be viewed at wileyonlinelibrary.com]

with a much smaller magnitude, and the winter season (January–February), when precipitation is predominantly brought by western disturbances, lacks a diurnal cycle altogether. In contrast, the pre-monsoon season (February–May) has an altogether different diurnal cycle: it is unimodal, with a much broader peak around the late afternoon and early evening. Precipitation during these months is typically brought by isolated convective events that take longer to build up than during the monsoon, due to the more stable, drier atmosphere (Shrestha *et al.*, 2012).

We also stratify the study region by latitude (not shown), to test whether the mean diurnal cycle changes significantly as a function of elevation—approximately a monotonic function of latitude over the study region. The amplitude of the cycle decreases with elevation, as does the relative magnitude of the nocturnal peak, but the bimodal structure of the cycle is retained at all latitudes, so we can be sure the signal is robust and representative.

To start to untangle the processes responsible for these peaks, and their variability, we look at composite daily data, split according to the timing of peak precipitation. We do this for anomalous precipitation over north India and the surrounding region in Figure 5. These composite diurnal cycles each have a distinct, unimodal peak, varying in magnitude between 1 and 2 mm hr^{-1}, and contributions from events not associated with the main peak are largely reduced (see, e.g., the suppressed nocturnal precipitation in the 0900–1200 IST composite). Associated precipitation anomalies have a footprint much larger than the study region itself, often spanning several hundred kilometres. Combined with the presence of distinct peaks, this implies that day-to-day variability of larger-scale conditions is responsible for modulating the timing of the diurnal cycle, even if the driving mechanisms themselves are localised. Using the structure of the precipitation anomalies, we can start to speculate on what these sources of variability might be, as the spatial scale is consistent with an active BSISO, monsoon trough, or monsoon LPS.

3.2 | Synoptic-scale drivers

To explore these structures in more detail, we extract days associated with the two diurnal peaks and construct vertical-meridional cross-section composites through the middle of the study region, (82.5°E) but extending further north (32.5°N) and south (22.5°N). Figure 6 shows this for days in which the diurnal peak occurs between 1200 and 1500 IST, and between 0000 and 0300 IST. The anomalies for each field are computed relative to the daily mean for each subset—that is, the sum of the four panels in each of (a) and (b) is zero. The two sets of days share many common features: the diurnal cycle of solar heating and radiative cooling of the surface and boundary layer results in a pair of counterflowing jets in the valley between the foothills and the Deccan Plateau (the high

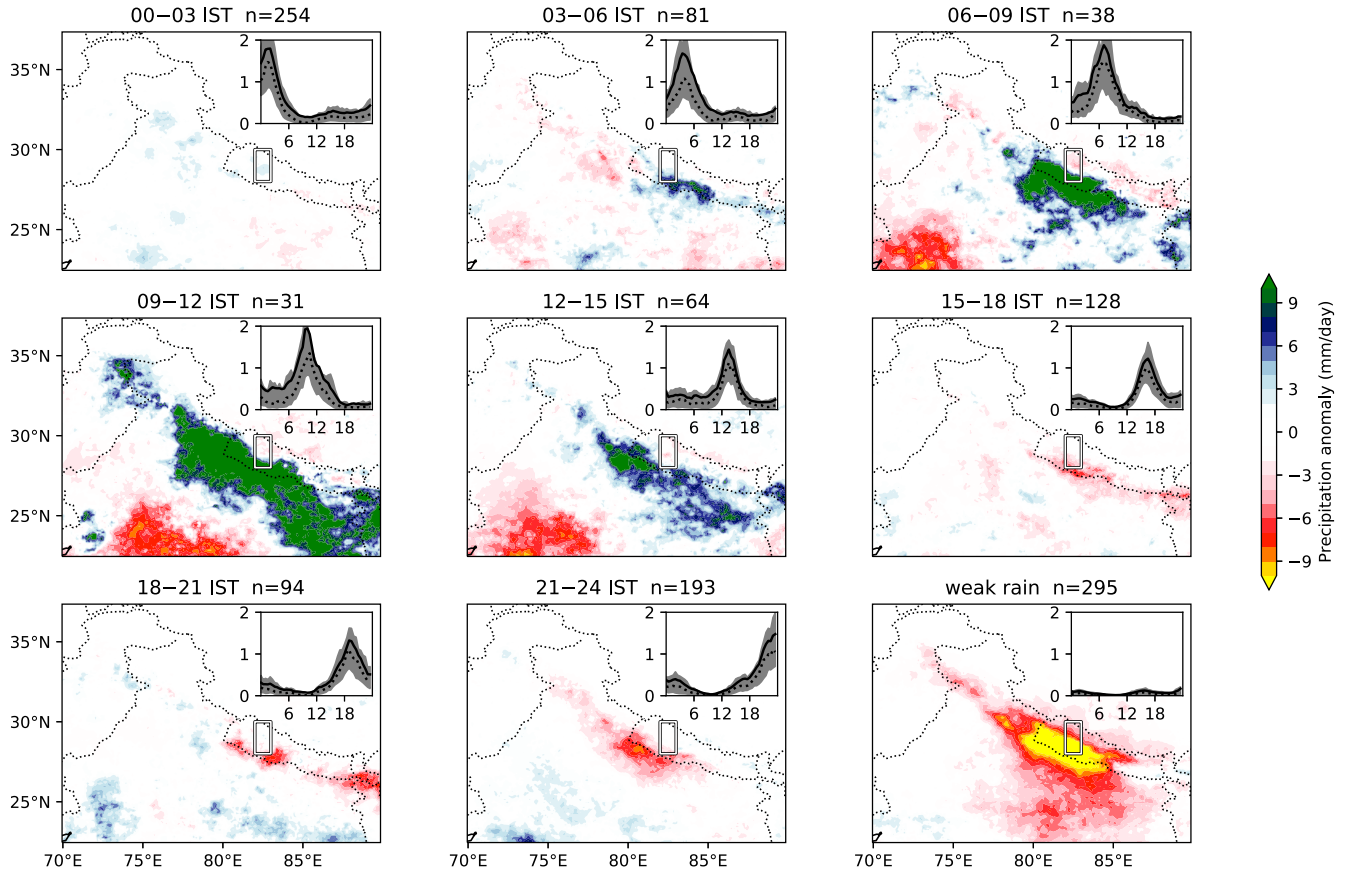

FIGURE 5 Composite anomalous daily precipitation, stratified by the timing of the peak of the diurnal cycle in the study region (marked by a white rectangle). The number of days included in each composite is given in the panel title. Composites are constructed thus: mean daily precipitation (0000–0000 IST) is computed over the study region for days in July and August during the available *GPM*–IMERG period (2000–2020). Days with precipitation in the lowest quartile are then separated and labelled as "weak rain". Remaining days are then categorised according to the timing of peak precipitation in the study region, binned into three-hourly groups, and composited. Inset are the mean (black line), median (dotted line), and interquartile range (grey) of the composite IST diurnal cycles of precipitation (mm hr^{-1}) for each subset, computed over the study region. Anomalies are computed relative to the mean of days not included in "weak rain". Uses *GPM*–IMERG data from July and August 2000–2020[Colour figure can be viewed at wileyonlinelibrary.com]

tableland south of the Gangetic Plain, covering most of Central and South India) that reverse direction semidiurnally, consistent with results from an idealised numerical model (de Wekker *et al.*, 1998). The most significant difference between the two sets of days is the timing of ascending moisture flux on the slopes. Upslope, ascent is strongly tied to diurnal heating, with the maximum occurring consistently at 1800 IST; however, further downslope, over our study region, the maximum upward vertical moisture flux occurs near, or slightly before, the time of maximum precipitation. This happens even though the reanalysis still prefers nocturnal precipitation, even on days in which late-afternoon precipitation is observed in *GPM*–IMERG. The strong ascent at 1200 IST in Figure 6a is supported by continued surface heating through 1800 IST. The boundary layer subsequently cools (0000 IST), through either evaporative cooling by precipitation or increased cloud cover. Either way, this results in increased stability and a more stable lower troposphere along the slopes, suppressing any later nocturnal precipitation. This explains why days on which afternoon precipitation occurs over the study region do not then continue to rain the following early morning, which is supported by the behaviour of ERA5 precipitation in Figure 6b, where a positive bias in afternoon precipitation comes at the cost of a negative bias in early-morning precipitation. A brief caveat here: these composites use pressure-level data, and so near-surface katabatic and anabatic winds and related density currents may not be represented appropriately. This will be addressed later.

This inspection of the diurnal cycle is informative, but does not offer much to help us understand the large-scale differences in atmospheric conditions that drive the competing mechanisms. Therefore, in Figure 7, which otherwise has identical construction to Figure 6, we take the anomalies relative to the time of day over the

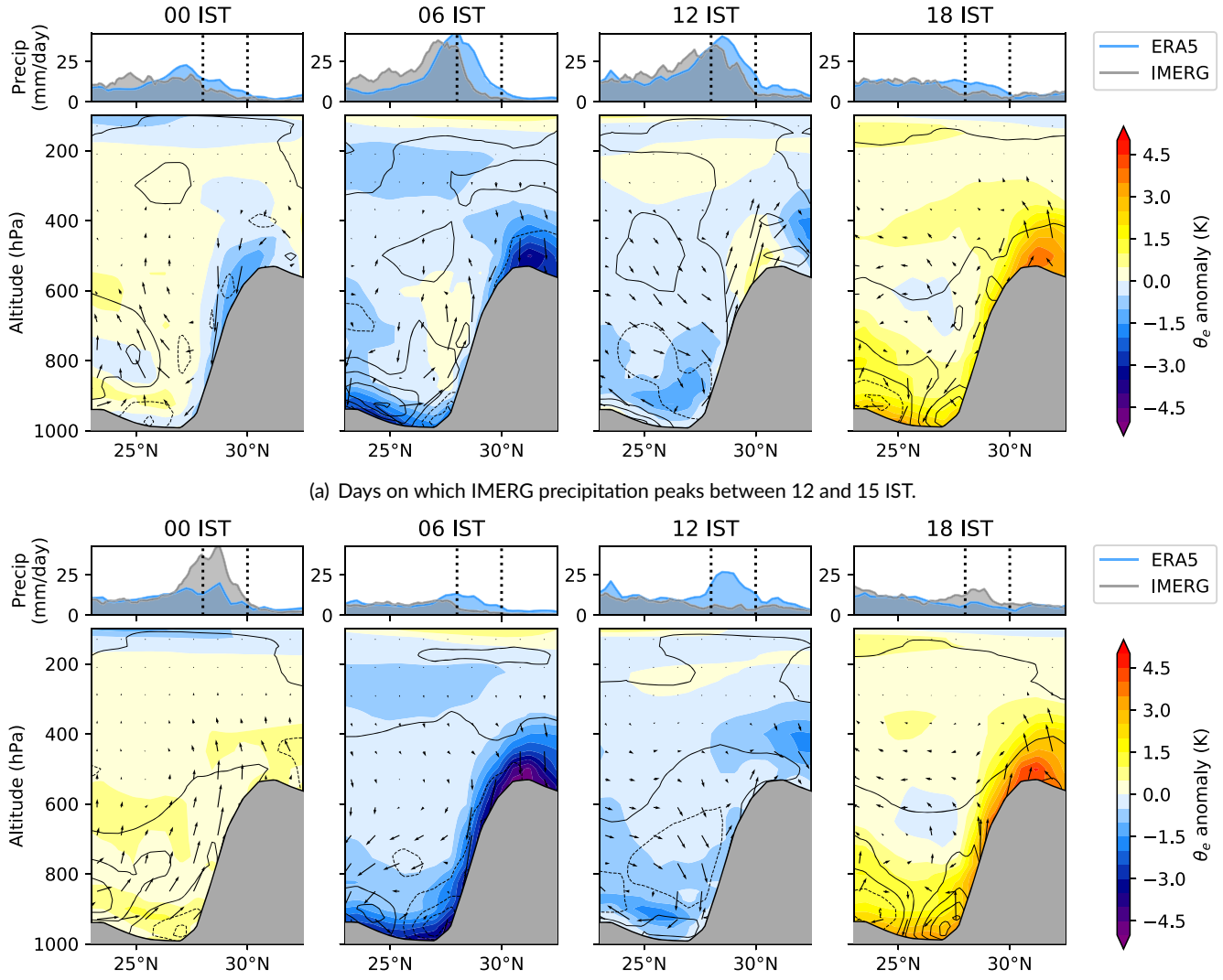

FIGURE 6 Diurnal cycle of selected instantaneous variables, shown as a cross-section through 82.5°E for days on which peak precipitation in the study region occurred (a) between 1200 and 1500 IST, and (b) between 0000 and 0300 IST. Meridional–vertical cross-sections show anomalous equivalent potential temperature (coloured contours, K), anomalous moisture flux normal to the cross-sectional plane (line contours in intervals of 5 g kg^{-1} m s^{-1}, solid lines indicate westerly flow, dashed lines easterly), and anomalous moisture flux parallel to the cross-sectional plane (arrows, vertical exaggerated 200×). Anomalies are computed relative to the daily mean. Computed using ERA5 data (2000–2018). Above each panel, on the same meridional axis, mean precipitation rate (ERA5: blue, *GPM*–IMERG: grey) over the next six hours (e.g., over 0000–0600 IST in the first panel) is plotted. Dotted lines show the study region (28–30°N)[Colour figure can be viewed at wileyonlinelibrary.com]

full July–August climatology. For example, fields plotted at 1200 IST have the 1200 IST climatology subtracted from them, which has the effect of removing the mean diurnal cycle. In this way, we can draw out the differences between the two subsets without the signal being swamped by diurnal variability.

The most striking difference between the two sets of cycles is the presence of a low-level jet. This is distinct from the nocturnal jet in Figure 6, and its scale is indicative of synoptic, rather than local, forcing. This anomalous moisture flux is centered at around 900 hPa, but extends up through to the mid-troposphere. It is westerly for days with peak precipitation between 1200 and 1500 IST and easterly for days with peak precipitation between 0000 and 0300 IST. This pattern extends over the whole set of peaks (not shown): days with peak precipitation between 1200 and 0000 IST are associated with easterly anomalous moisture flux south of the foothills, whereas days with peak precipitation between 0000 and 1200 IST are associated with westerly moisture flux. There is a thermal response to, and hence secondary circulation associated with, this jet. For example, the anomalous westerly jet present on days with

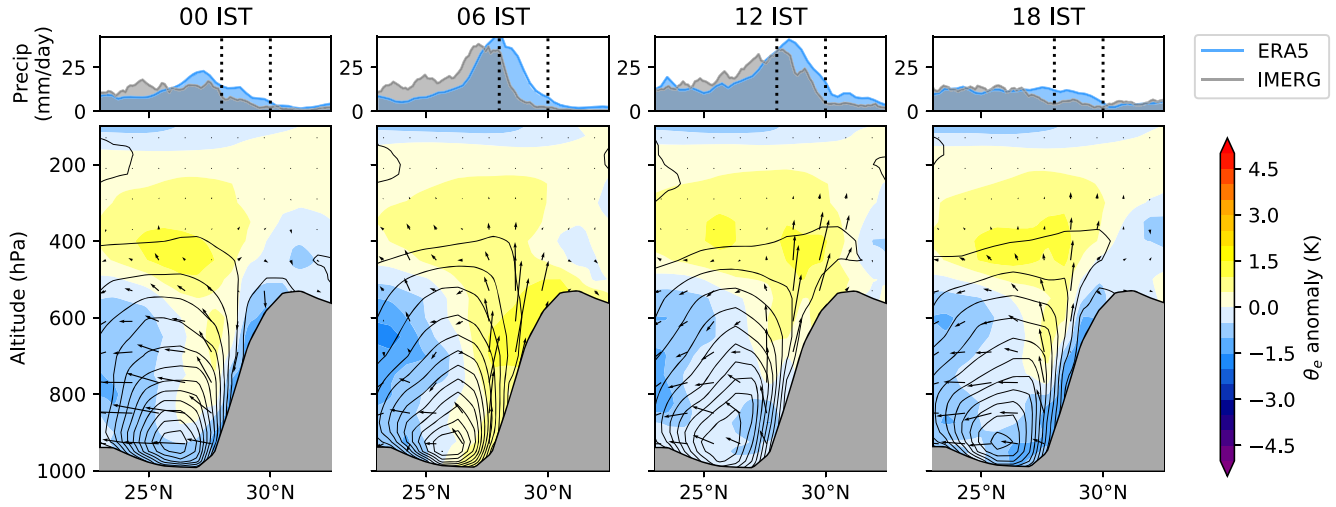

(a) Days on which IMERG precipitation peaks between 12 and 15 IST.

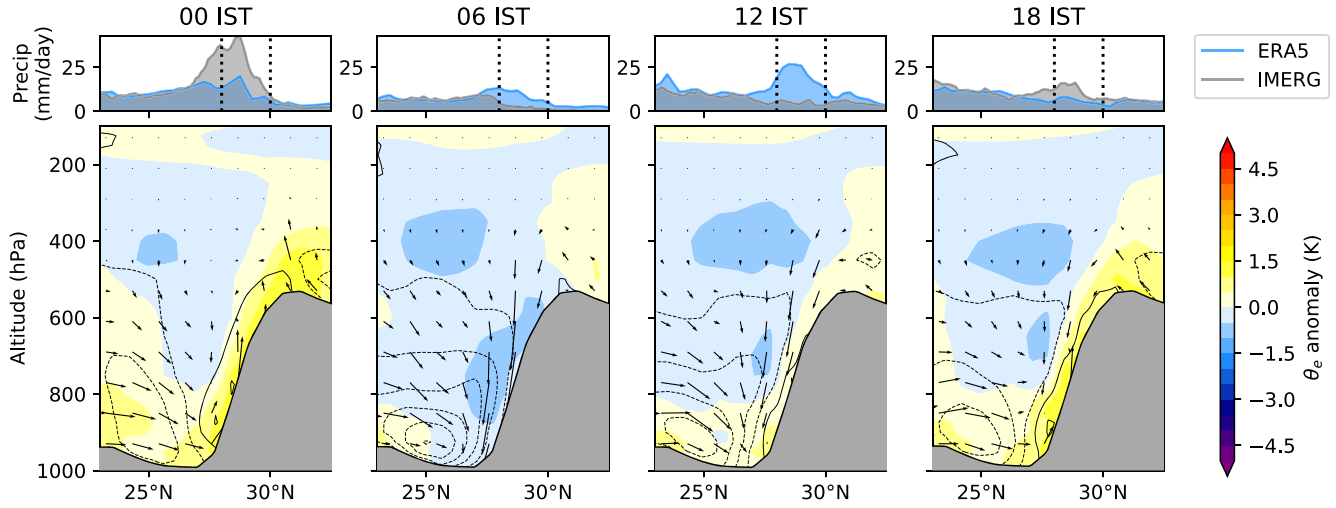

(b) Days on which IMERG precipitation peaks between 00 and 03 IST.

FIGURE 7 As Figure 6, except anomalies are computed relative to the same time of day over all days. For example, the 1800 IST composite is shown as an anomaly to the 1800 IST July–August mean[Colour figure can be viewed at wileyonlinelibrary.com]

daytime peaks is balanced by a positive meridional gradient in θ_e; the secondary circulation thus provides moisture and updrafts to the foothills, supporting the usual diurnal cycle of tropical convection (peaking during the local afternoon). In contrast, the easterly jet is associated with large-scale downdrafts over the region, suppressing canonical tropical convection and generally supporting nocturnal katabatic flow. We will explore these features on the synoptic scale in Figure 8.

To explore the synoptic-scale conditions responsible for supporting these anomalous jets, we again partition days according to Figure 4: those with peak precipitation between 0000 and 0300 IST are considered "nocturnal" peak days, and those with peak precipitation between 1200 and 1500 IST are considered "daytime" peak days. Compositing daily vertical wind speed and 750-hPa winds for each and computing the anomaly with respect to a July–August climatology (Figure 8) shows that the two groups are associated with significantly different monsoon conditions. Nocturnal peak days are associated with a deepening of the monsoon trough, weak increased ascent over the head of the Bay of Bengal and monsoon core zone, and slightly reduced ascent (or increased descent) along the foothills due to barrier flow effects, consistent with Figure 7b. The reverse is true for daytime peak days: an anomalously weak trough allows synoptic-scale anomalous westerlies to impinge on the Himalaya, with the subsequent forced ascent supporting large-scale deep convection. The composite difference of these synoptic conditions is consistent with either an active spell of the monsoon or the passage of a monsoon low-pressure system. We will explore this hypothesis further in Section 3.3.

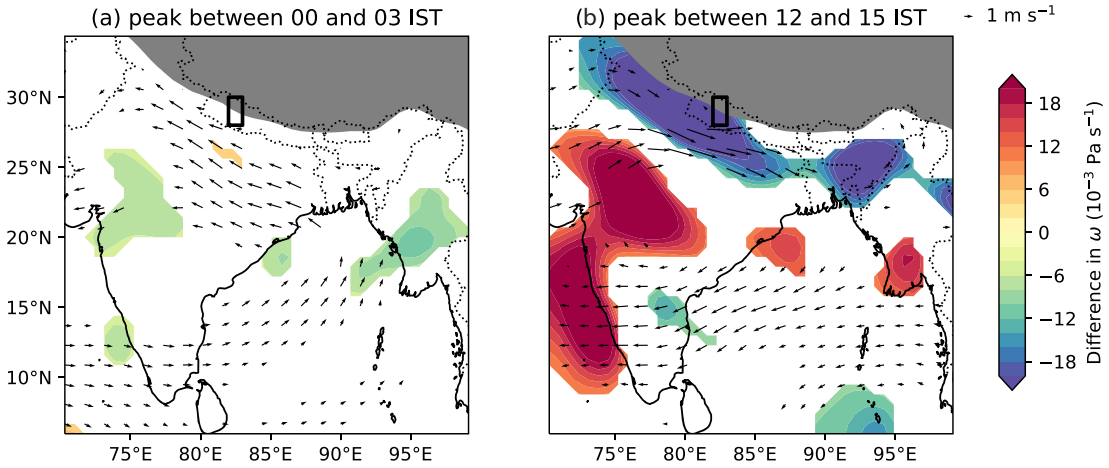

FIGURE 8 Composite anomalous daily mean 750-hPa horizontal winds (arrows) and vertical wind speed (coloured contours, negative values indicate ascent) for (a) days on which peak precipitation in the study region (marked with a black rectangle) occurs between 0000 and 0300 IST and (b) days on which it occurs between 1200 and 1500 IST. Days with weak precipitation (lowest quartile) are not included in these subsets. The anomaly is computed against the July–August 2000–2018 climatology. Areas where climatological surface pressure is less than 750 hPa are greyed out. Data are masked where the composites do not differ significantly from the climatology at a 95% confidence level. Computed using ERA5 data (2000–2018)[Colour figure can be viewed at wileyonlinelibrary.com]

To complete our understanding of the diurnal cycle, we must ask how these two driving processes—deep convection supported by synoptic-scale flow, and the more localised katabatic flow—project on to it. Are they actually coupled to the cycle, and does this coupling change meaningfully between days with different precipitation peak timing? We can explore these relationships in detail by examining the phase space of the composite diurnal cycle for different sets of days. Figure 9 shows the mean diurnal cycles of 10-m v (a proxy for katabatic flow), vertically integrated moisture flux convergence (VIMFC, a proxy for large-scale deep convection), and precipitation, averaged over the study area. Two sets of days are included, representing the two local peaks in Figure 4: those with peak precipitation occurring between 1200 and 1500 IST and those where it occurs between 0000 and 0300 IST.

The two sets of days present markedly different composite diurnal cycles in this phase space. On the daytime peak days (1200–1500 IST), mean VIMFC peaks at 3.6×10^{-4} kg·m^{-2}·s^{-1} at about 1400 IST, remaining high for several hours. The peak precipitation immediately follows this event. In contrast, on nocturnal peak days (0000–0300 IST), the VIMFC peak is much shorter and weaker, reaching only 2.5×10^{-4} kg·m^{-2}·s^{-1}. This means that much less moisture is available for deep convection in the afternoon and, as a result, very little precipitation occurs at this time. This is corroborated (not shown) by the composite diurnal cycle of 500-hPa ω.

We can also see the relative importance of the low-level cross-slope winds. Climatologically, these are slightly upslope (positive 10-m v) because of the orientation of the monsoon trough relative to the foothills; however, at night, as the katabatic effect reaches a maximum, these approach zero or even become negative. Here, the role of the large scale is again important: during nocturnal days, peak precipitation occurs as 10-m v approaches its lowest value, but this also coincides with an increase in VIMFC, suggesting that in such cases the katabatic flow is interacting with the monsoon environment at the north edge of the trough to produce moisture convergence along the slope. During daytime peak days, there is no simultaneous increase in VIMFC at this time, and hence no heavy precipitation. So, while the katabatic and convective processes are the primary drivers for the two sets of peaks, they do not operate entirely independently. In the same way, we see in Figure 9 how the convective peak may be further supported by anabatic winds. These feedbacks are complementary to the mechanism proposed by Barros and Lang (2003), who found that daytime precipitation over Nepal was favoured during periods where strong anabatic flow prevented the build up of moisture convergence in the lower foothills.

3.3 | Response to intraseasonal forcing

3.3.1 | The relationship between convective organisation and the diurnal cycle

In the rest of this study, we will dedicate ourselves to understanding the drivers behind the convective processes that cause precipitation to fall over the Central Himalaya during the local afternoon or early evening. There are

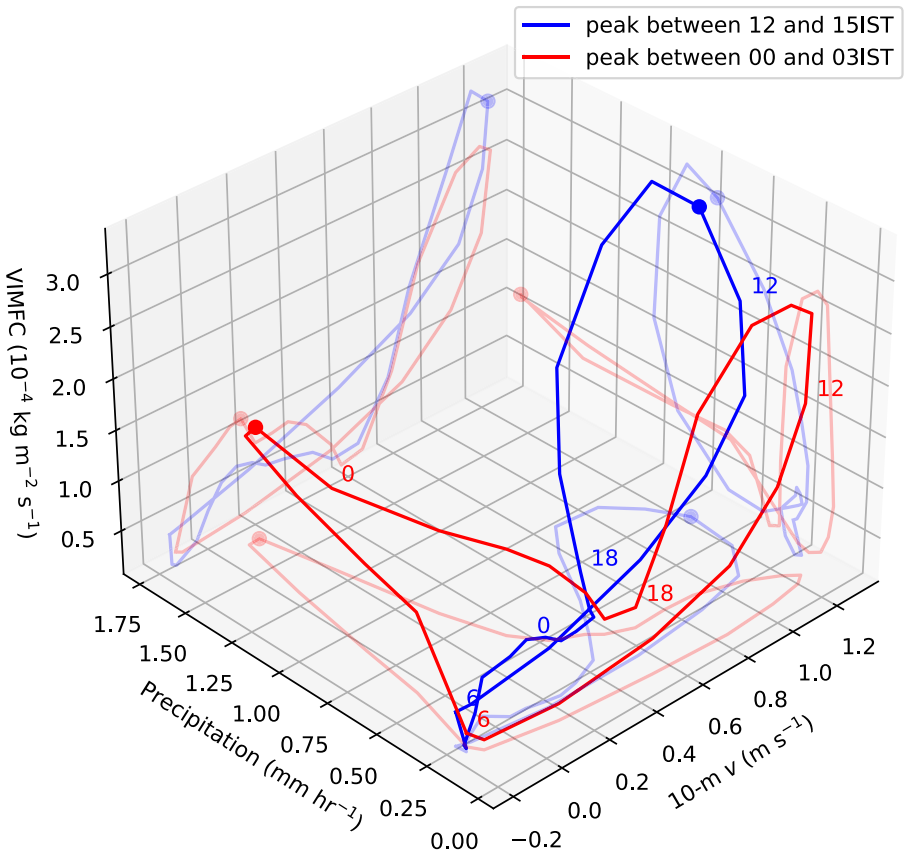

FIGURE 9 Three-dimensional phase space showing the relationship between cross-slope surface flow, vertically integrated moisture flux convergence, and precipitation over the course of the diurnal cycle. Composited for days on which peak precipitation occurs between 1200 and 1500 IST (blue) and 0000 and 0300 IST (red). Bullets indicate the mean time of peak precipitation, and additional numerical markers indicate the local (IST) time of day for each cycle. The pale sets of red and blue lines show the projection of the cycle on to the three respective axis planes. Computed using ERA5 (VIMFC and 10-m *v*) and *GPM*–IMERG (precipitation)[Colour figure can be viewed at wileyonlinelibrary.com]

several reasons for this focus. Firstly, as we saw in the Introduction, the katabatic processes over this region are generally well understood. Secondly, daytime precipitation over this region is the exception rather than the rule, and so it is important to quantify potential sources of variability, particularly given the challenge of simulating the diurnal cycle of convection in the Tropics (Watters *et al.*, 2021).

We start by exploring the structure and variability of deep convection itself over the region surrounding the Central Himalaya. Using *Kalpana* satellite OLR data, we located contiguous regions of deep convection by identifying 0.25° × 0.25° pixels where OLR<167 W·m^{-2} at each three-hourly timestep. Regions were then categorised jointly according to their area and the fraction of the study region they covered. Composite precipitation for the twelve sets of bins (except for very small storms covering more than one third of the study region, for which there were no cases) is shown in Figure 10, along with the diurnal cycle for each type and the fraction of daytime (1200–2100 IST) precipitation for which that category is responsible. The total attributable fraction is 55.5%, and this would likely be higher still if we used a more relaxed threshold for identifying convection, or a higher resolution OLR product capable of resolving more isolated deep convection. In contrast, only about 30% of nocturnal precipitation can be explained in this way.

Contributions come from a range of different sizes of storm. The smallest ($\leq$6,250 km^2; length-scale $\lesssim$80 km) are associated with 14.0% of afternoon and early-evening precipitation (1200–2100 IST: i.e., the window when convective peaks are most common) over the study region. They provide heavy precipitation to a small area and follow the typical diurnal cycle of convection closely, peaking at 1700 IST and decaying over the next few hours. Medium-sized storms (6,250 < $A \leq$ 62,500 km^2; length-scale between ~80 and ~250 km) contribute 15.4% of the daytime precipitation. Medium-sized storms that are further south, and thus cover only a small fraction of the box (top panel), have a diurnal cycle largely consistent with tropical convection, but those that are further north and cover much more of the region (bottom panel) have a much flatter diurnal cycle, suggesting that the convective and katabatic modes are mixed at this scale: although the storms are highly convective, either a subset are being triggered by katabatic flow, or they are being intensified by katabatic convergence once mature.

The scale of the storm that the katabatic mode can generate is limited by both the length-scale of the orography and the ability of these storms to aggregate given the available environmental shear. Thus, our category of large storms (62,500 < $A \leq$ 625,000 km^2; length-scale between ~250 km and ~800 km) is quite unlikely to be triggered

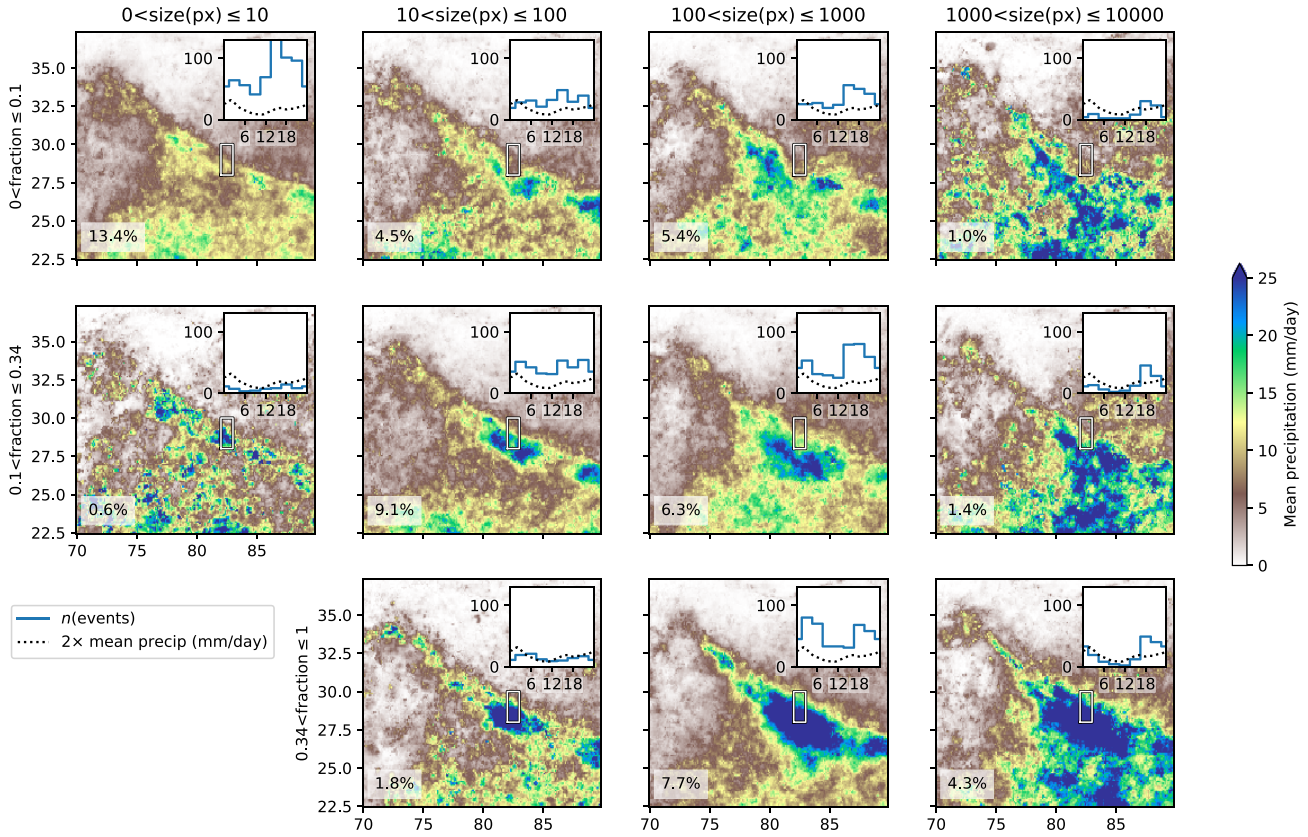

FIGURE 10 The relationship between convective organisation and the diurnal cycle. Convective regions are identified in *Kalpana* OLR data as any contiguous area in the domain (50–100°W, 0–40°N) with OLR< 167 W·m^{-2}. Any convective regions that overlap the study region (white rectangle) are then binned in columns according to their area (measured in 0.25 ×0.25°, approximately 625 km^2, pixels), and in rows according to the fraction of study area covered. For any timestep where more than one storm overlaps the study region, we consider only the largest. Composite mean precipitation is given for each pair of bins, with the diurnal cycle of event frequency inset (blue). Given in the inset, for comparison, is the mean diurnal cycle of precipitation (scaled for clarity) over the study region for Jul–Aug (dotted line). The fraction of total July–August 1200–2100 IST precipitation that occurs during each subset is given in the lower left of the respective panel. Precipitation data from *GPM*–IMERG[Colour figure can be viewed at wileyonlinelibrary.com]

orographically. These storms account for more daytime precipitation (19.4%) than any other size, and the mean diurnal cycle of their frequency peaks at 1700–1900 IST. This peak occurs a few hours later in storms that are further north (bottom panel), suggesting that they may have initiated to the south and then propagated into the region. The high-coverage subset also has a second peak at 0200 IST, which we hypothesize is due to intensification from low-level moisture flux convergence caused by katabatic flow. The largest category of storm (> 625,000 km^2; length-scale greater than ~800 km) is comparatively rare, but still contributes nearly 7% of the daytime precipitation to the region, having a well-defined peak in frequency at 1800 IST. The peak is broadest (i.e., the decay is slowest) for systems covering most of the box, again highlighting the role of local orographically driven dynamics in supporting large-scale storms that arrive over the region.

Our discussion on the footprints of deep convection led to four conclusions: (a) deep convection contributes the majority of daytime precipitation over the Central Himalaya, (b) regardless of scale, it typically follows the canonical diurnal cycle of tropical convection, peaking at around 1800 IST, with exceptions (c) when propagating northward from the trough, in which case it occurs over the foothills several hours later, or (d) when residual storms are intensified at night through interactions with local orographic dynamics. We saw that the precipitation contributed was roughly equal across the three smaller size bins (15–20%) and a bit less for the largest size (7%). However, the synoptic conditions differ considerably between environments favourable for small-scale and large-scale convection. At the smaller end, intraseasonal variability tends to be controlled by the BSISO and monsoon active/break cycles; whereas at the larger end, convection is typically organised by low-pressure systems. We will now quantify the effect of each of these flavours of intraseasonal variability on the diurnal cycle of precipitation over the Central Himalaya.

3.3.2 | The BSISO

We start with the BSISO, often thought of as the meridionally propagating component of the Madden–Julian Oscillation (MJO). It is associated with northwest–southeast bands of positively or negatively anomalous OLR propagating northward across India and Southeast Asia, with a frequency of 10–60 days (Lee *et al.*, 2013). Like the MJO, the BSISO is defined using the phase relationship between two principal-component time series, and is thus quantified using both a phase (from 1 to 8) and a standardised magnitude. Both the diurnal cycle and the BSISO are "circular" variables in this regard, but simply computing a direct circular correlation between the two is not appropriate, because it relies on the assumption that the two variables covary somewhat uniformly. This may not be the case: the two peaks on the diurnal cycle, which are almost opposite in phase, could be strongly associated with neighbouring BSISO phases, but, unless the relationship with the remaining phases is consistently ordered, the correlation would be low despite plausible causality. We must take a more nuanced approach. To do this, we compute the mean diurnal cycle for each BSISO phase at each grid point. Then, by taking the standard deviation of the amplitude of those eight cycles and the circular standard deviation (see Section 2.2.2) of the eight peak times, we can identify regions where the BSISO affects the timing and amplitude of the diurnal cycle of precipitation appreciably: in regions where the standard deviations are low, the relationship is weak; where the standard deviation is high, the relationship is strong. To quantify uncertainty, we do this for both *GPM*–IMERG and ERA5, the latter of which should capture intraseasonal variability well over the Central Himalaya, as it does over the Western Himalaya (Baudouin *et al.*, 2020).

The BSISO has almost no effect on the timing of the diurnal cycle of ERA5 precipitation over the study region, and only has a comparatively weak effect on IMERG (Figure 11). There is also only a relatively weak effect on the cycle amplitude: the magnitude of the convective (1600 IST) peak averaged over the box only varies from 0.35 to 0.47 $mm \cdot hr^{-1}$ between the different BSISO phases (lowest in phase 4; highest in phase 8). The magnitude of the nocturnal peak varies between 0.57 and 0.88 $mm \cdot hr^{-1}$ (lowest in phase 4; highest in phase 5). These are in broad agreement with the behaviour of the BSISO, for which negative OLR anomalies reach their furthest north in phase 5 and there are significant positive OLR anomalies over the Central Himalaya during phase 4. In summary, while the BSISO can affect the magnitude of the convective and katabatic peaks to some extent, it is not enough to invert the population so that the convective peak is stronger than the katabatic peak for any given phase. This may be because the BSISO does not propagate sufficiently far north: we see in both IMERG and ERA5 that it does have a substantial effect on the timing and amplitude of the diurnal cycle further south, over the Indo-Gangetic Plain, a topic that we leave for further research.

3.3.3 | Low-pressure systems

Finally, we look at the role of monsoon low-pressure systems (LPSs), which are capable of inducing extended periods of large-scale moisture flux, organised deep convection, and deepening/extending of the monsoon trough. Convective activity is most sensitive to their location rather than intensity (Hunt *et al.*, 2021), and so in Figure 12 we bin LPS tracks on to a $1° \times 1°$ grid and compute the mean diurnal cycle over the study region for the dates included in each box, as long as at least 10 LPSs were present. When LPSs are either in the centre or the south of the trough, or are located far away from the Himalaya (e.g., over Sri Lanka or the Arabian Sea), the peak of the mean diurnal cycle remains close to the katabatic peak at about 0300 IST. Where LPSs are at the northern edge of the trough, or extend it to the northwest, the convective peak becomes stronger and the peak of the mean diurnal cycle moves to the afternoon (1500 IST), consistent with the larger storm sizes of Figures 8 and 10. One possible reason for this is the cloud structure of LPSs: Hunt *et al.* (2016) showed that monsoon depressions (their figure 5) are often associated with deep convective cloud near their centre and stratiform cloud at larger radii. Thus, an LPS in the centre of the trough provides moisture, but not much convective instability to the foothills, supporting the katabatic peak, whereas an LPS further north may cause deep convection to occur directly over the study region. Further work is needed to explore how LPSs interact with the orography over the Central Himalaya.

4 | DISCUSSION

Before concluding, we will briefly discuss some of the caveats and implications of this work in a modelling framework. Perhaps the most important caveat is basing many of our results on the interpretation of reanalysis data. At a horizontal resolution of ~25 km, many of the valleys that may be providing the more intense katabatic flow are not represented. Figure 13 shows the mean diurnal cycle and frequency of peak timing over the study region for *GPM*–IMERG, ERA5, and two simulations of the 2016 monsoon season in the Met Office Unified Model (MetUM) at horizontal resolutions of 17 km (parametrised convection) and 4.4 km (explicit convection), conducted

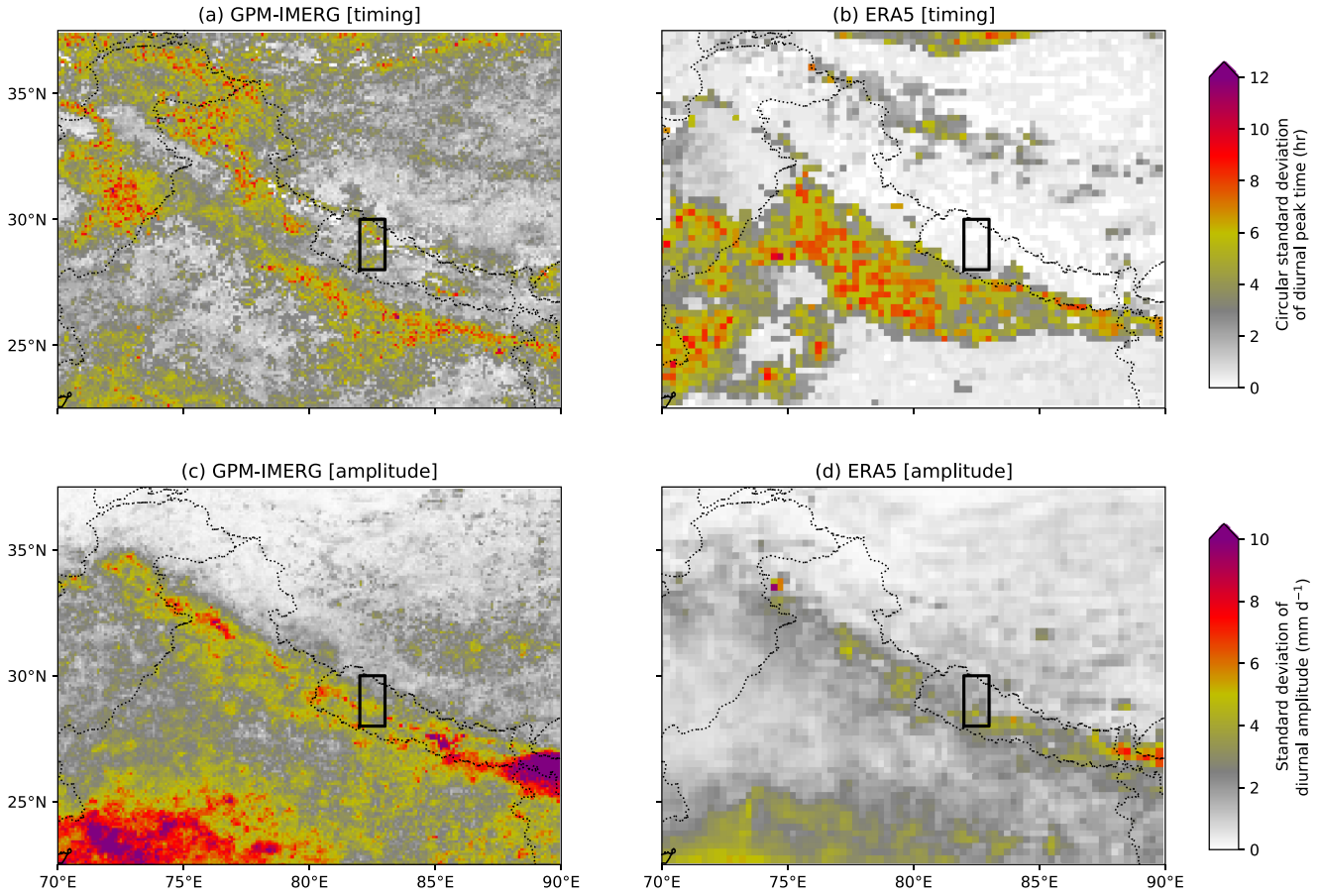

FIGURE 11 Effect of the BSISO on (a,b) timing and (c,d) amplitude of the diurnal peak. The mean diurnal cycle for each BSISO phase is computed at each grid point. The circular standard deviation of the peak timing and the standard deviation of the cycle amplitude are then computed. Low values in (a) and (b) suggest that the BSISO has little or no impact on the timing of the diurnal peak. The study region is marked with a black rectangle[Colour figure can be viewed at wileyonlinelibrary.com]

as part of the INCOMPASS previous project (Turner *et al.*, 2020). We also include another reanalysis, IMDAA (Rani *et al.*, 2021), which has higher horizontal resolution (12 km) than ERA5 and uses a version of the MetUM as its driving model. To confirm that the statistics for a single season are valid, both the climatology (dotted) and the 2016 season (solid) are plotted for the reanalyses and satellite data. In the reanalyses and 17-km MetUM experiment, we can also partition the precipitation into "convective" (produced by the convection scheme) and "stratiform" (produced by the microphysics scheme).

Both reanalyses and the 17-km experiment capture the convective and katabatic peaks, but overestimate the magnitude of the convective peak and significantly underestimate the magnitude of the katabatic peak. The coarsest model (ERA5) underestimates this peak the most, and the highest-resolution model (IMDAA) the least, which may imply that fine representation of orography is crucial to correct representation of the katabatic winds (and thus to the nocturnal moisture convergence required for the precipitation). Moisture not used up as precipitation during the katabatic peak is then available later for the convective peak. It is a helpful sanity check to see that the contribution of convective precipitation is much larger during the convective peak than the katabatic peak, where stratiform precipitation plays a more significant role, even overtaking the convective contribution in ERA5. Understanding the respective strengths (e.g., both peaks present and at approximately the right time) and weaknesses (e.g., the relative strengths of the peaks are inconsistent with observation) of these parametrised-convection models is left for future work. The convection-permitting 4.4-km experiment is beset by a different problem. The convection takes too long to build up during the day, since uplifting an entire 4.4-km grid box requires a lot of instability. This means that the convective peak is very broad and can occur very late (1500–2000 IST). The katabatic peak also occurs too late (0400–0500 IST), and the amplitude of the cycle is weakened by more constant precipitation. Norris *et al.* (2017) showed that the diurnal cycle varied strongly as a function of elevation in their convection-permitting simulation of the Central Himalaya. We find this to a small extent over

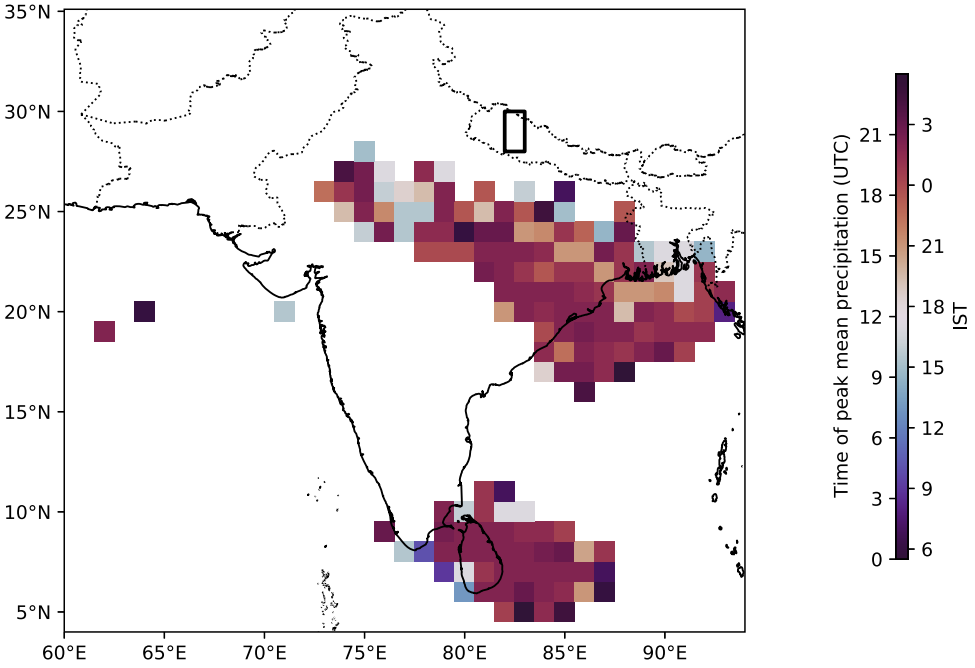

FIGURE 12 The effect of LPS presence on the timing of the diurnal cycle of precipitation over the study region. Track points of LPSs (2000–2018) are binned into a 1° × 1° grid. Grid points with at least 10 days of LPS overpasses are then coloured according to the peak timing of the mean diurnal cycle over the study region[Colour figure can be viewed at wileyonlinelibrary.com]

the study region (not shown). The diurnal cycle remains bimodal between 28° and 29.5°N, though the katabatic peak occurs earlier at higher elevation, going from 0700 IST at 28°N to 0100 IST at 30°N. The convective peak is similarly broad and late at all latitudes, except north of 29.5°N, where it is absent altogether. Neither of these elevation-dependent features is present in *GPM*–IMERG (not shown). It is therefore likely that this would be at least partially improved by models with subkilometre resolution (e.g., Yashiro *et al.*, 2016), where convection is resolved rather than just permitted and where the representation of the orography is fine enough to capture the valleys responsible for strong pulses of katabatic flow, but we leave such an assessment for future work.

5 | CONCLUSIONS

In this study, we have explored the complex diurnal cycle of precipitation over the monsoonal Central Himalaya. Using a small study region that we believe to be representative (82–83°E, 28–30°N), we showed that the mean diurnal cycle has two broad peaks, one during the late afternoon (1700 IST) and one during the early morning (0200 IST). The early-morning peak has the greater magnitude in the mean cycle during July and August, but this pattern reverses during the pre- and post-monsoon months of June and September, when the late-afternoon peak has the greater magnitude.

Reanalyses and a 17-km model with parametrised convection broadly capture both peaks, but overestimate the magnitude of the afternoon peak while underestimating the magnitude of the early-morning peak. Simple diagnostics that just compute the timing of the maximum of the mean diurnal cycle are thus insufficient to validate model performance in this region—simply comparing the peak times of the climatological mean diurnal cycles would point to a phase bias of about ten hours here, which is an incomplete and exaggerated description of the actual biases.

We showed that this bimodal cycle is an artefact of compositing: individual days are usually associated with a single peak that typically lasts for several hours and may occur at any time, although most frequently during the early morning and late afternoon. Both peaks are associated with a significant low-level nocturnal jet, which can therefore be ruled out as a significant moisture source that preferentially supports one or the other.

We confirmed previous studies that showed that the early-morning peak was due to katabatic winds interacting with the mean monsoon flow to drive moisture flux convergence along the foothills. We hypothesize that this explains why this peak is comparatively weaker outside the monsoon, and that underestimating the magnitude of the katabatic wind due to coarse orographic representation is a potential source of the bias in models and reanalyses. Further work is needed to connect these results to the hypothesis of Fitzjarrald (1984), whereby early-morning convection in the Himalayan foothills is triggered by the gravity-wave response of the mountains blocking monsoon flow, and to the results of Medina *et al.* (2010), who attributed differences in the morphology of convective storms across the Himalaya to the differing diurnal cycles of surface heat fluxes. Similarly, further work is needed

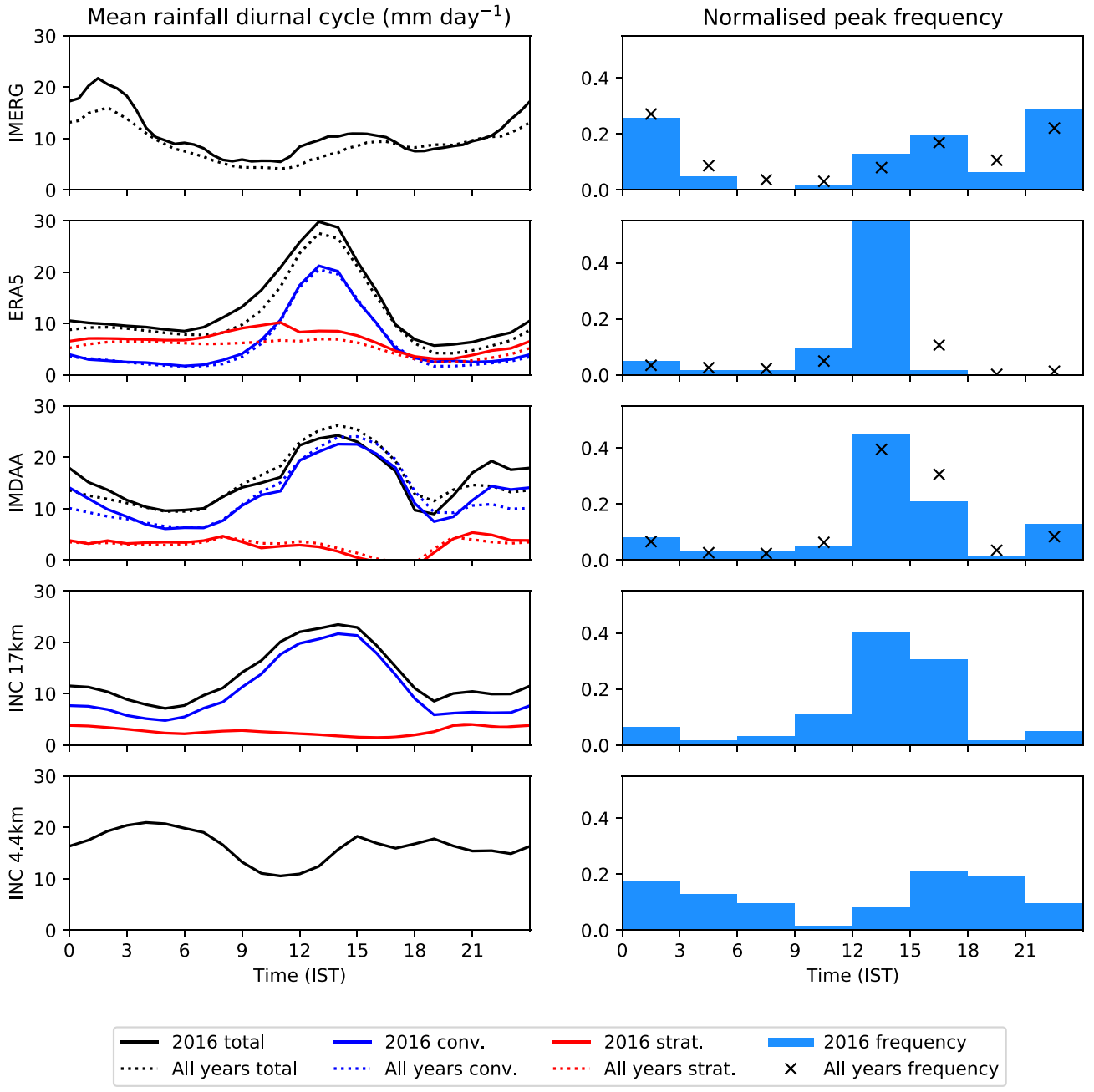

FIGURE 13 Comparison of diurnal cycle of precipitation over the study region in *GPM*–IMERG, ERA5, and IMDAA reanalyses, and two resolutions (17 km with parametrised convection; 4.4 km with explicit convection) of a limited-area MetUM experiment simulating the 2016 season. Left: the mean Jul–Aug diurnal cycle (for 2016 with solid lines, for all available years with dotted lines), with convective (blue) and large-scale (red) contributions if available. Right: the relative frequency of days with a diurnal peak occurring in the given three-hourly bins is plotted (2016 with blue bars, all available years with black crosses)[Colour figure can be viewed at wileyonlinelibrary.com]

to explore exactly why afternoon precipitation is so rare on days with a nocturnal peak, despite a large afternoon maximum in moisture flux convergence.

We showed that the late-afternoon peak is linked to the canonical diurnal cycle of tropical convection, and that the convection responsible occurs at a range of scales ranging from tens (small mesoscale convective systems) to thousands (monsoon low-pressure systems) of kilometres. We found that systems present after midnight could be intensified further at low altitudes by katabatic flow. We hypothesize that anabatic flow may assist in intensifying or triggering convection at higher altitudes during the daytime.

We explored a range of sources of intraseasonal variability, finding only very weak relationships between the BSISO and the diurnal cycle, and between the monsoon

active/break phases and the diurnal cycle. We also found, however, that monsoon LPSs, when sufficiently far north or west, significantly favoured the convective peak.

ACKNOWLEDGEMENTS

KMRH, AGT, and RK.H.S. are funded through the Weather and Climate Science for Service Partnership (WCSSP) India, a collaborative initiative between the Met Office, supported by the UK Government's Newton Fund, and the Indian Ministry of Earth Sciences (MoES). R.K.H.S. is also supported by the National Centre for Atmospheric Sciences.

AUTHOR CONTRIBUTIONS

Kieran M. R. Hunt: conceptualization; formal analysis; investigation; methodology; visualization; writing – original draft. **Andrew G. Turner:** funding acquisition; project administration; supervision; writing – review and editing. **Reinhard K. H. Schiemann:** project administration; supervision; writing – review and editing.

ORCID

Kieran M. R. Hunt https://orcid.org/0000-0003-1480-3755

Andrew G. Turner https://orcid.org/0000-0002-0642-6876

REFERENCES

Ahrens, B., Meier, T. and Brisson, E. (2020) Himalayan Weather and Climate and their Impact on the Environment. In: *Diurnal Cycle of Precipitation in the Himalayan Foothills–Observations and Model Results*: Heidelberg: Springer.

Arulalan, T., AchutaRao, K., Hunt, K.M.R., Turner, A.G., Mitra, A.K. and Sarkar, A. (2020) Prediction of western disturbances tracks using NEPS. https://www.ncmrwf.gov.in/event/emmda/Abstracts/TArulalan_Abstract_EMMDA.pdf. accessed 25 October 2021.

Barros, A.P., Joshi, M., Putkonen, J. and Burbank, D.W. (2000) A study of the 1999 monsoon rainfall in a mountainous region in central Nepal using TRMM products and rain gauge observations. *Geophysical Research Letters*, 27, 3683–3686.

Barros, A.P., Kim, G., Williams, E. and Nesbitt, S.W. (2004) Probing orographic controls in the Himalayas during the monsoon using satellite imagery. *Natural Hazards and Earth System Sciences*, 4, 29–51.

Barros, A.P. and Lang, T.J. (2003) Monitoring the monsoon in the Himalayas: observations in central Nepal, June 2001. *Monthly Weather Review*, 131, 1408–1427.

Baudouin, J.-P., Herzog, M. and Petrie, C.A. (2020) Cross-validating precipitation datasets in the Indus River basin. *Hydrology and Earth System Sciences*, 24, 427–450.

Bhatt, B.C. and Nakamura, K. (2006) A climatological–dynamical analysis associated with precipitation around the southern part of the Himalayas. *Journal of Geophysical Research*, 111, D02115.

Bluestein, H.B. (1993) *Synoptic–Dynamic Meteorology in Midlatitudes. Volume II. Observations and Theory of Weather Systems*, (p. 392). New York, NY: Oxford University Press.

Bollasina, M., Bertolani, L. and Tartari, G. (2002) Meteorological observations at high altitude in the Khumbu Valley, Nepal Himalayas, 1994–1999. *Bulletin of Glaciological Research*, 19, 1–12.

Dai, A. and Trenberth, K.E. (2004) The diurnal cycle and its depiction in the Community Climate System Model. *Journal of Climate*, 17, 930–951.

Dezfuli, A.K., Ichoku, C.M., Huffman, G.J., Mohr, K.I., Selker, J.S., Van De Giesen, N., Hochreutener, R. and Annor, F.O. (2017) Validation of IMERG precipitation in Africa. *Journal of Hydrometeorology*, 18, 2817–2825.

Dirmeyer, P.A., Cash, B.A., Kinter, J.L., Jung, T., Marx, L., Satoh, M., Stan, C., Tomita, H., Towers, P., Wedi, N., Achuthavarier, D., Adams, J.M., Altshuler, E.L., Huang, B., Jin, E.K. and Manganello, J. (2012) Simulating the diurnal cycle of rainfall in global climate models: resolution versus parameterization. *Climate Dynamics*, 39, 399–418.

Dong, W.-H., Ming, Y. and Ramaswamy, V. (2020) Projected changes in South Asian monsoon low-pressure systems. *Journal of Climate*, 33(17), 7275–7287. https://doi.org/10.1175/JCLI-D-20-0168.1

Egger, J., Bajrachaya, S., Egger, U., Heinrich, R., Reuder, J., Shayka, P., Wendt, H. and Wirth, V. (2000) Diurnal winds in the Himalayan Kali Gandaki valley. Part I: observations. *Monthly Weather Review*, 128, 1106–1122.

Fisher, N.I. (1995) *Statistical Analysis of Circular Data*. Cambridge: Cambridge University Press.

Fitzjarrald, D.R. (1984) Katabatic wind in opposing flow. *Journal of Atmospheric Sciences*, 41, 1143–1158.

Hersbach, H., Bell, B., Berrisford, P., Hirahara, S., Horányi, A., Muñoz-Sabater, J., Nicolas, J., Peubey, C., Radu, R., Schepers, D., Simmons, A., Soci, C., Abdalla, S., Abellan, X., Balsamo, G., Bechtold, P., Biavati, G., Bidlot, J., Bonavita, M., De Chiara, G., Dahlgren, P., Dee, D., Diamantakis, M., Dragani, R., Flemming, J., Forbes, R., Fuentes, M., Geer, A., Haimberger, L., Healy, S., Hogan, R.J. and Hólm, E. (2020) The ERA5 global reanalysis. *Quarterly Journal of the Royal Meteorological Society*, 146, 1999–2049.

Hou, A.Y., Kakar, R.K., Neeck, S., Azarbarzin, A.A., Kummerow, C.D., Kojima, M., Oki, R., Nakamura, K. and Iguchi, T. (2014) The global precipitation measurement mission. *Bulletin of the American Meteorological Society*, 95, 701–722.

Houze, R.A., Wilton, D.C. and Smull, B.F. (2007) Monsoon convection in the Himalayan region as seen by the TRMM Precipitation Radar. *Quarterly Journal of the Royal Meteorological Society*, 133, 1389–1411. https://doi.org/10.1002/qj.106.

Huffman, G.J., Bolvin, D.T. and Nelkin, E.J. (2015) Integrated Multi-satellitE Retrievals for GPM (IMERG) technical documentation. *NASA/GSFC Code*, 612, 2019.

Hunt, K.M.R. and Fletcher, J.K. (2019) The relationship between Indian monsoon rainfall and low-pressure systems. *Climate Dynamics*, 53, 1–13.

Hunt, K.M.R., Turner, A.G. and Parker, D.E. (2016) The spatiotemporal structure of precipitation in Indian monsoon depressions. *Quarterly Journal of the Royal Meteorological Society*, 142, 3195–3210. https://doi.org/10.1002/qj.2901.

Hunt, K.M.R., Turner, A.G., Stein, T.H.M., Fletcher, J.K. and Schiemann, R.K.H. (2021) Modes of coastal precipitation over southwest India and their relationship with intraseasonal variability. *Quarterly Journal of the Royal Meteorological Society*, 147, 181–201.

Joyce, R.J., Janowiak, J.E., Arkin, P.A. and Xie, P. (2004) CMORPH: a method that produces global precipitation estimates from passive microwave and infrared data at high spatial and temporal resolution. *Journal of Hydrometeorology*, 5, 487–503.

Kikuchi, K. and Wang, B. (2008) Diurnal precipitation regimes in the global tropics. *Journal of Climate*, 21, 2680–2696.

Kozu, T., Kawanishi, T., Kuroiwa, H., Kojima, M., Oikawa, K., Kumagai, H., Okamoto, K., Okumura, M., Nakatsuka, H. and Nishikawa, K. (2001) Development of precipitation radar on board the Tropical Rainfall Measuring Mission (TRMM) satellite. *IEEE Transactions on Geoscience and Remote Sensing*, 39, 102–116. https://doi.org/10.1109/36.898669.

Kummerow, C., Barnes, W., Kozu, T., Shiue, J. and Simpson, J. (1998) The Tropical Rainfall Measuring Mission (TRMM) sensor package. *Journal of Atmospheric and Oceanic Technology*, 15, 809–817. https://doi.org/10.1175/1520-0426(1998)015<0809:TTRMMT>2.0.CO;2.

Kummerow, C., Simpson, J., Thiele, O., Barnes, W., Chang, A.T.C., Stocker, E., Adler, R.F., Hou, A., Kakar, R., Wentz, F., Ashcroft, P., Kozu, T., Hong, Y., Okamoto, K., Iguchi, T., Kuroiwa, H., Im, E., Haddad, Z., Huffman, G., Ferrier, B., Olson, W.S., Zipser, E., Smith, E.A., Wilheit, T.T., North, G., Krishnamurti, T. and Nakamura, K. (2000) The status of the Tropical Rainfall Measuring Mission (TRMM) after two years in orbit. *Journal of Applied Meteorology*, 39, 1965–1982. https://doi.org/10.1175/1520-0450(2001)040<1965:TSOTTR>2.0.CO;2.

Lee, J.-Y., Wang, B., Wheeler, M.C., Fu, X., Waliser, D.E. and Kang, I.-S. (2013) Real-time multivariate indices for the boreal summer intraseasonal oscillation over the Asian summer monsoon region. *Climate Dynamics*, 40, 493–509.

Mahakur, M., Prabhu, A., Sharma, A.K., Rao, V., Senroy, S., Singh, R. and Goswami, B.N. (2013) A high-resolution outgoing longwave radiation dataset from Kalpana-1 satellite during 2004–2012. *Current Science*, 105(8), 1124–1133.

Marsham, J.H., Dixon, N.S., Garcia-Carreras, L., Lister, G.M.S., Parker, D.J., Knippertz, P. and Birch, C.E. (2013) The role of moist convection in the West African monsoon system: insights from continental-scale convection-permitting simulations. *Geophysical Research Letters*, 40, 1843–1849.

Martin, G.M., Brooks, M.E., Johnson, B., Milton, S.F., Webster, S., Jayakumar, A., Mitra, A.K., Rajan, D. and Hunt, K.M.R. (2020) Forecasting the monsoon on daily to seasonal time-scales in support of a field campaign. *Quarterly Journal of the Royal Meteorological Society*, 146, 2906–2927.

Medina, S., Houze, R.A., Jr, Kumar, A. and Niyogi, D. (2010) Summer monsoon convection in the Himalayan region: terrain and land cover effects. *Quarterly Journal of the Royal Meteorological Society*, 136, 593–616.

Nesbitt, S.W. and Zipser, E.J. (2003) The diurnal cycle of rainfall and convective intensity according to three years of TRMM measurements. *Journal of Climate*, 16, 1456–1475. https://doi.org/10.1175/1520-0442%282003%29016%3C1456%3ATDCORA%3E2.0.CO%3B2.

Norris, J., Carvalho, L.M.V., Jones, C. and Cannon, F. (2020) Warming and drying over the central Himalaya caused by an amplification of local mountain circulation. *Nature Climate and Atmospheric Science*, 3, 1–11.

Norris, J., Carvalho, L.M.V., Jones, C., Cannon, F., Bookhagen, B., Palazzi, E. and Tahir, A.A. (2017) The spatiotemporal variability of precipitation over the Himalaya: evaluation of one-year WRF model simulation. *Climate Dynamics*, 49, 2179–2204.

Pfeifroth, U., Trentmann, J., Fink, A.H. and Ahrens, B. (2016) Evaluating satellite-based diurnal cycles of precipitation in the African tropics. *Journal of Applied Meteorology and Climatology*, 55, 23–39.

Prakash, S., Mitra, A.K., AghaKouchak, A., Liu, Z., Norouzi, H. and Pai, D.S. (2018) A preliminary assessment of GPM-based multisatellite precipitation estimates over a monsoon dominated region. *Journal of Hydrology*, 556, 865–876.

Rani, S.I., Arulalan, T., George, J.P., Rajagopal, E.N., Renshaw, R., Maycock, A., Barker, D.M. and Rajeevan, M. (2021) IMDAA: high-resolution satellite-era reanalysis for the Indian monsoon region. *Journal of Climate*, 34, 5109–5133.

Romatschke, U. and Houze, R.A. Jr (2011) Characteristics of precipitating convective systems in the South Asian monsoon. *Journal of Hydrometeorology*, 12, 3–26.

Romatschke, U., Medina, S. and Houze, R.A. (2010) Regional, seasonal, and diurnal variations of extreme convection in the South Asian region. *Journal of Climate*, 23, 419–439.

Rüthrich, F., Thies, B., Reudenbach, C. and Bendix, J. (2013) Cloud detection and analysis on the Tibetan Plateau using Meteosat and CloudSat. *Journal of Geophysical Research: Atmospheres*, 118, 10–82.

Sahany, S., Venugopal, V. and Nanjundiah, R.S. (2010) Diurnal-scale signatures of monsoon rainfall over the Indian region from TRMM satellite observations. *Journal of Geophysical Research: Atmospheres*, 115, D02103. https://doi.org/10.1029/2009JD012644.

Sen Roy, S. and Balling, R.C. Jr (2007) Diurnal variations in summer season precipitation in India. *International Journal of Climatology: A Journal of the Royal Meteorological Society*, 27, 969–976.

Sharma, N., Attada, R. and Hunt, K.M.R. (2021). Evaluating winter precipitation over the western Himalayas in high resolution Indian regional reanalysis using multi-source climate datasets. In prep.

Shrestha, D., Singh, P. and Nakamura, K. (2012) Spatiotemporal variation of rainfall over the central Himalayan region revealed by TRMM Precipitation Radar. *Journal of Geophysical Research: Atmospheres*, 117, D22106. https://doi.org/10.1029/2012JD018140.

Singh, R., Thapliyal, P.K., Kishtawal, C.M., Pal, P.K. and Joshi, P.C. (2007) A new technique for estimating outgoing longwave radiation using infrared window and water vapor radiances from Kalpana very high resolution radiometer. *Geophysical Research Letters*, 34, L23815.

Tang, G.-Q., Clark, M.P., Papalexiou, S.M., Ma, Z.-Q. and Hong, Y. (2020) Have satellite precipitation products improved over last two decades? A comprehensive comparison of GPM IMERG with nine satellite and reanalysis datasets. *Remote Sensing of Environment*, 240, 111697.

Turner, A.G., Bhat, G.S., Martin, G.M., Parker, D.J., Taylor, C.M., Mitra, A.K., Tripathi, S.N., Milton, S., Rajagopal, E.N., Evans, J.G., Morrison, R., Pattnaik, S., Sekhar, M., K. Bhattacharya, B.K., Madan, R., Govindankutty, M., Fletcher, J.K., Willetts, P.D., Menon, A., Marsham, J.H. and INCOMPASS Team

(2020) Interaction of convective organisation with monsoon precipitation, atmosphere, surface and sea: the 2016 INCOMPASS field campaign in India. *Quarterly Journal of the Royal Meteorological Society*, 146, 2828–2852.

Ueno, K., Kayastha, R.B., Yasunari, T., Nakawo, M. and Chitrakar, M.R. (2001) Meteorological observations during 1994–2000 at the automatic weather station (GEN-AWS) in Khumbu region, Nepal Himalayas. *Bulletin of Glaciological Research*, 18, 23–30.

Wallace, J.M. (1975) Diurnal variations in precipitation and thunderstorm frequency over the conterminous United States. *Monthly Weather Review*, 103, 406–419.

Watters, D., Battaglia, A. and Allan, R.P. (2021) The diurnal cycle of precipitation according to multiple decades of global satellite observations, three CMIP6 models, and the ECMWF reanalysis. *Journal of Climate*, 34, 5063–5080.

de Wekker, S.F.J., Zhong, S., Fast, J.D. and Whiteman, C.D. (1998) A numerical study of the thermally driven plain-to-basin wind over idealized basin topographies. *Journal of Applied Meteorology and Climatology*, 37, 606–622.

Yang, G.-Y. and Slingo, J. (2001) The diurnal cycle in the Tropics. *Monthly Weather Review*, 129, 784–801.

Yashiro, H., Kajikawa, Y., Miyamoto, Y., Yamaura, T., Yoshida, R. and Tomita, H. (2016) Resolution dependence of the diurnal cycle of precipitation simulated by a global cloud-system resolving model. *Sola*, 12, 272–276.

How to cite this article: Hunt, K. M. R., Turner, A. G. & Schiemann, R. K. H. (2022) Katabatic and convective processes drive two preferred peaks in the precipitation diurnal cycle over the Central Himalaya. *Quarterly Journal of the Royal Meteorological Society*, 1–21. Available from: https://doi.org/10.1002/qj.4275